Automatic identification of hypertension and assessment of its secondary effects using artificial intelligence: A systematic review (2013–2023)

Computers in Biology and Medicine 172 (2024) 108207

Contents lists available at ScienceDirect

Computers in Biology and Medicine

journal homepage: www.elsevier.com/locate/compbiomed

Automatic identification of hypertension and assessment of its secondary effects using artificial intelligence: A systematic review (2013–2023)

Anjan Gudigar [a], Nahrizul Adib Kadri [b], U. Raghavendra [a,*], Jyothi Samanth [c], M. Maithri [d], Mahesh Anil Inamdar [d], Mukund A. Prabhu [e], Ajay Hegde [f], Massimo Salvi [g], Chai Hong Yeong [h], Prabal Datta Barua [i,j,k], Filippo Molinari [g], U. Rajendra Acharya [l,m]

[a] Department of Instrumentation and Control Engineering, Manipal Institute of Technology, Manipal Academy of Higher Education, Manipal, 576104, India
[b] Department of Biomedical Engineering, Faculty of Engineering, University of Malaya, Kuala Lumpur, 50603, Malaysia
[c] Department of Cardiovascular Technology, Manipal College of Health Professions, Manipal Academy of Higher Education, Manipal, 576104, India
[d] Department of Mechatronics, Manipal Institute of Technology, Manipal Academy of Higher Education, Manipal, 576104, India
[e] Department of Cardiology, Kasturba Medical College, Manipal Academy of Higher Education, Manipal, 576104, India
[f] Manipal Hospitals, Bengaluru, Karnataka, 560102, India
[g] Biolab, PolitoBIOMedLab, Department of Electronics and Telecommunications, Politecnicodi Torino, Turin, Italy
[h] School of Medicine, Faculty of Health and Medical Sciences, Taylor's University, 47500, Subang Jaya, Malaysia
[i] Cogninet Brain Team, Cogninet Australia, Sydney, NSW, 2010, Australia
[j] School of Business (Information Systems), Faculty of Business, Education, Law & Arts, University of Southern Queensland, Toowoomba, QLD, 4350, Australia
[k] Faculty of Engineering and Information Technology, University of Technology Sydney, Sydney, NSW, 2007, Australia
[l] School of Mathematics, Physics, and Computing, University of Southern Queensland, Springfield, QLD, 4300, Australia
[m] Centre for Health Research, University of Southern Queensland, Toowoomba, QLD, 4350, Australia

ARTICLE INFO

Keywords:
Artificial intelligence
Clinical data
Deep learning
Hypertension
Physiological signals
Imaging modalities
Machine learning

ABSTRACT

Artificial Intelligence (AI) techniques are increasingly used in computer-aided diagnostic tools in medicine. These techniques can also help to identify Hypertension (HTN) in its early stage, as it is a global health issue. Automated HTN detection uses socio-demographic, clinical data, and physiological signals. Additionally, signs of secondary HTN can also be identified using various imaging modalities. This systematic review examines related work on automated HTN detection. We identify datasets, techniques, and classifiers used to develop AI models from clinical data, physiological signals, and fused data (a combination of both). Image-based models for assessing secondary HTN are also reviewed. The majority of the studies have primarily utilized single-modality approaches, such as biological signals (e.g., electrocardiography, photoplethysmography), and medical imaging (e.g., magnetic resonance angiography, ultrasound). Surprisingly, only a small portion of the studies (22 out of 122) utilized a multi-modal fusion approach combining data from different sources. Even fewer investigated integrating clinical data, physiological signals, and medical imaging to understand the intricate relationships between these factors. Future research directions are discussed that could build better healthcare systems for early HTN detection through more integrated modeling of multi-modal data sources.

1. Introduction

Hypertension (HTN) generally known as high Blood Pressure (BP) is a main health condition affecting 1.28 billion adults aged between 30 and 79 years, of which two-thirds are in low-middle-income countries.[1] HTN is one of the common causes of cardiovascular and neurological complications such as heart failure, stroke, myocardial infarction, and other vascular diseases. Similarly, HTN in an advanced stage affects other vital organs and produces renal failure and retinopathy [1,2]. Fig. 1 demonstrates the major complications of HTN affecting the vital organs.

It has been documented that heart failure and stroke were the major causes of death in HTN patients [3]. HTN is defined as repeat office Systolic Blood Pressure (SBP) and Diastolic Blood Pressure (DBP)

* Corresponding author.
E-mail address: raghavendra.u@manipal.edu (U. Raghavendra).

[1] https://www.who.int/news-room/fact-sheets/detail/hypertension, accessed on November 23, 2023.

https://doi.org/10.1016/j.compbiomed.2024.108207
Received 27 December 2023; Received in revised form 9 February 2024; Accepted 12 February 2024
Available online 28 February 2024

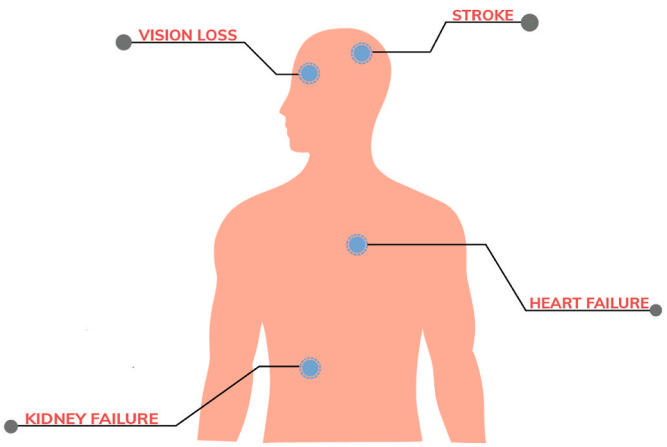

Fig. 1. Major organs that are commonly affected by long-term uncontrolled high blood pressure.

measurements exceeding 140 and 90 mmHg respectively [1]. HTN is generally categorized into primary (essential) HTN and secondary HTN. Primary HTN reflects aortic vascular changes mediated by the renin-angiotensin-aldosterone system that regulates the BP, peripheral cardiac autonomic regulation system, nitric oxide, and natriuretic peptide [4–6]. Secondary HTN is found in small proportions which display specific causes for the HTN such as genetic causes, metabolic changes, renal artery stenosis, middle aortic syndrome, and coarctation of the aorta, etc. Further, HTN is classified into different grades depending on systolic and DBP readings. Table 1 displays the HTN classification based on BP recording [7]. Clinically HTN is the most heterogenous disease, where most of them remain asymptomatic and left undiagnosed. Yet few patients may experience headache, giddiness, breathlessness, bleeding in the nose, and palpitation as initial presenting signs of HTN, which are not specific but can demonstrate the severe form of HTN when present [8,9]. Diagnostic and management goals in HTN mainly target the confirmation of the diagnosis of HTN and the presence of end-organ damage secondary to HTN. Managing the HTN with an achievable BP control has a very high impact on clinical prognosis and prevents fatal complications.

BP measurement stands as an imperative step in the diagnosis and evaluation of HTN. Once elevated BP recording is confirmed with at least 3 serial measurements, HTN patients are then worked up to identify the causes of HTN and to evaluate the end-organ damage caused by HTN. Although multiple noninvasive techniques have been proven to be reliable tests of choice in the evaluation of HTN, central aortic BP measure in cardiac catheterization demonstrates the real-time BP waveforms with the most accurate value [10,11]. Several important aspects are assessed during the medical history of HTN patients. This includes collecting a brief personal history and evaluating risk factors for cardiovascular conditions. The history also looks for present or past symptoms of diseases like Cardiovascular Disease (CVD), Hypertensive Mediated Organ Damage (HMOD), stroke, renal disease, and possible secondary causes of HTN. Lastly, history enquires about any non-HTN drug being used, as these could impact a patient's condition. Physical examination focuses on body habitus to look for biophysical profiles, signs of any HMOD, and signs of secondary HTN. Biophysical profile includes weight, height, Body Mass Index (BMI), obesity, etc. Examination for signs of HMOD emphasizes neurological evaluation, fundoscopic examination, cardiac auscultation, carotid artery examination, and ankle-brachial index. Additionally, signs of secondary HTN are demonstrated by skin inspection, palpation of the kidney, auscultation of cardiac and renal vessels for murmur, signs of Cushing's disease, and signs of thyroid disease. Besides, selected standard laboratory tests of blood and urine samples are necessary in the initial work-up for HTN patients [12–14].

Table 1
Categorization of HTN based on office BP measurement [7].

Category	Systolic BP (mm Hg)	Diastolic BP (mm Hg)
Normal	<130	<85
High -Normal (pre-hypertension)	130–139	85–89
Grade 1 HTN	140–159	90–99
Grade 2 HTN	≥160	≥100
Isolated systolic HTN	≥140	<90
Isolated diastolic HTN	<140	≥90

HTN requires thorough evaluation as HTN patients exhibit a wide range of clinical and medical findings. Therefore, detection and continuous follow-up of HTN is still a challenging and open research area in developing countries with less proactive healthcare management systems. The application of Machine Learning (ML) techniques has enabled the detection of HTN using the clinical data available in Electronic Health Records (EHRs) [15,16]. Further, various physiological signals such as Electrocardiography (ECG), Photoplethysmography (PPG), etc., are used with feature extraction and ML techniques [17]. As a result, the obtained ML models are meant to support doctors or clinical experts to aid their clinical findings [18,19].

1.1. Assessment of HTN

In general, evaluation of HTN patients involves accurate measurement of BP, obtaining specific medical history, performing physical examination, and advising for routine laboratory investigations [20,21]. 12 lead ECG is also obtained invariably in HTN patients. A thorough evaluation of these features provides insights into the presence of HMOD, possible causes of HTN, and associated cardiovascular risk factors and sets the bassline value in the assessment of treatment effect [20–22]. According to Framingham's heart study criteria, (Coronary Artery Risk Development in Young Adults - CARDIA) clinical and biophysical profile of an individual such as age, gender, BMI, smoking habit, SBP reading and parental HTN history showed a better prediction model for new HTN than the presence of presystolic HTN [23,24]. Also, pulse wave velocity has been thought to be a potential mode in the prediction of future HTN among adults aged between 30 and 45 years [25].

Additionally, evaluation of HMOD is important in HTN cases, as the presence and extent of HMOD define the risk of development of CVD [26–28] Numerous tests and evaluation methods are used to assess HMOD. 12-lead ECG is used to assess cardiac rhythm, heart rate, and presence of Left Ventricular Hypertrophy (LVH). The ratio of urine albumin to creatinine can be used to screen and grade Chronic Kidney Disease (CKD). Blood serum creatinine level and estimated glomerular filtration rate also can be used to grade CKD. Further extended screening for HMOD requires multimodality assessment for damage to end organs such as the heart, kidney, brain, eye, great vessels, and peripheral arteries. Echocardiography is the most feasible noninvasive diagnostic test that evaluates cardiac structure and function. This helps in the screening for the presence of LVH, left ventricular systolic and diastolic function status, atrial size and function, valvular heart disease, and aortic aneurysm. Echocardiography is more sensitive than ECG in the detection of LVH [29,30].

Several tests can evaluate HTN-related organ damage. Brachial-ankle pulse wave velocity and carotid-femoral pulse wave velocity measure aortic vessel stiffness. Ultrasound (US) imaging of the carotid artery determines the plaque/stenosis and can be used to measure intima-media thickness. US screening of abdominal aorta helps diagnose abdominal aortic aneurysm in HTN patients. US imaging of the kidney depicts the size and structure of the kidney and helps in identifying renovascular disease and renal artery stenosis if present [31]. Spectral Doppler application in kidney US also assesses renal resistive index which is a marker of atherosclerosis and HMOD [32]. Fundoscopic

evaluation of the retina detects changes in the microvasculature. Further, HTN-mediated changes in the brain can be demonstrated by Magnetic Resonance Imaging (MRI) or Computed Tomography (CT). Often brain MRI depicts subtle cerebral changes that do not possess any clinical signs yet demonstrate a high risk for future adverse events. CT imaging can also be used to estimate the coronary calcium score, which provides intuition on coronary atherosclerosis.

A comprehensive evaluation of HTN patients considers several factors important for risk stratification, prognosis, and treatment decisions. BP readings, extent of HMOD, presence of additional cardiovascular risk factors, and existing HTN complications all provide insight into patient risk levels. Those with more severe or advanced diseases face poorer prognoses. Organ damage measures and complication status also influence whether more aggressive therapy is warranted. Therefore, accurately diagnosing and staging of HTN involves a multi-faceted assessment approach.

1.2. Motivation

Although HTN requires multisystem evaluation using multiple diagnostic and imaging modalities, it is important to follow a multidisciplinary approach. In this context, various imaging modalities encompass the clinical expertise and experience of the healthcare provider in each step. Hence developing an automated diagnostic modality using the spectrum of clinical data, signals and images derived from the various diagnostic modalities may support the clinicians in better diagnostic accuracy while evaluating the HTN patients. From the literature, it has been observed that many works have been reviewed and analyzed for the automatic detection of HTN using various risk factors based on sociodemographic [15,16] and physiological signals [17]. Martinez-Ríos et al. [18], surveyed the related works that use both approaches. However, automated methods combining multiple modalities for HTN monitoring have been under-explored. This review therefore aims to understand available evidence on multi-modal screening methods for the automated detection of HTN. The goal is to develop a more comprehensive picture drawing on the full range of relevant clinical, signal, and image-based information (see Fig. 2) to support clinicians through an integrated diagnostic tool.

It may be noted from Fig. 2 that our review compiles the works conducted on ML and DL approaches using clinical data, physiological signals, and various imaging modalities.

1.3. Computer Aided Diagnostic (CAD) tool

The manual detection of HTN and its assessment is a very challenging task. Thus CAD tools are developed to reduce human errors. Usually, the automated system on HTN is categorized into two divisions namely: i) identification or detection of HTN, and ii) assessment of its secondary effects.

Identification or detection of HTN: This involves using risk factors like BMI, gender, age, etc. to build prediction models with ML algorithms such as Artificial Neural Network (ANN) [33], Support Vector Machine (SVM) [34], Random Forest (RF) [35], etc. Another approach uses ECG and PPG signals to estimate BP values such as diastolic and systolic and applies ML for classification [17]. Some models fuse clinical data and physiological signals for improved prediction [36,37].

***Assessment of secondary effects*:** Imaging modalities help identify HTN's secondary structural effects on vital organs. For example, researchers use Magnetic Resonance Angiography (MRA) of the brain to classify images into hypertensive or normal groups using ANN [38]. Likewise, heart US is also used [39] with a feature reduction technique for the assessment of HTN. The assessment of the structural changes in human vital organs would help clinicians to predict the HTN before its onset. The complete automated system workflow is shown in Fig. 3. Detailed descriptions of each approach are provided in the following sections.

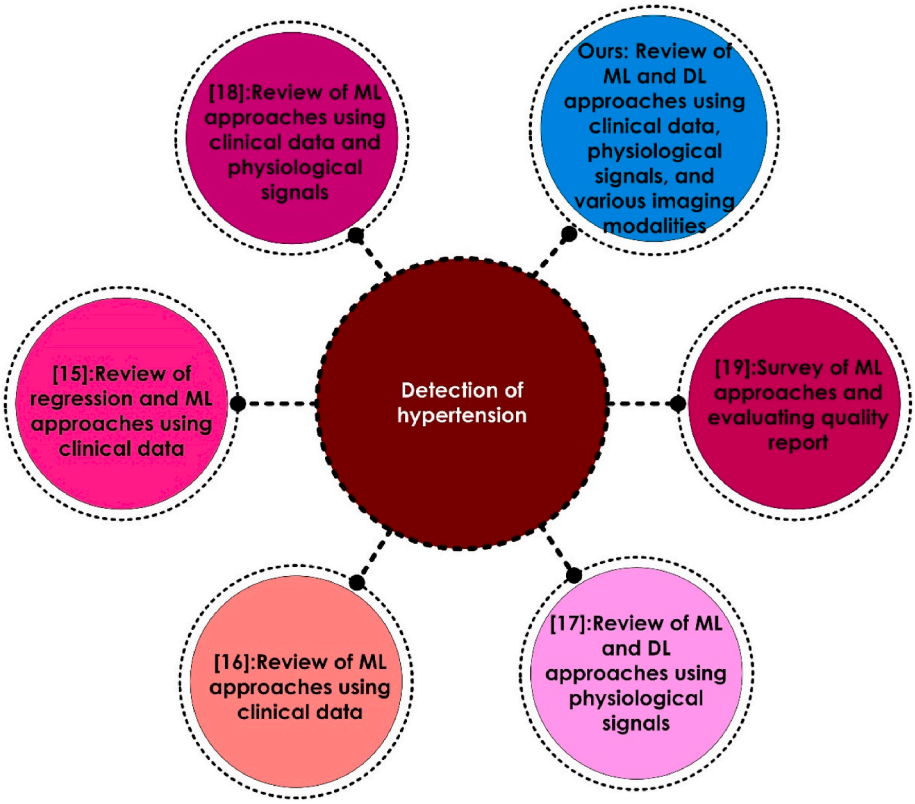

Fig. 2. Comparison of our review with other reviews conducted.

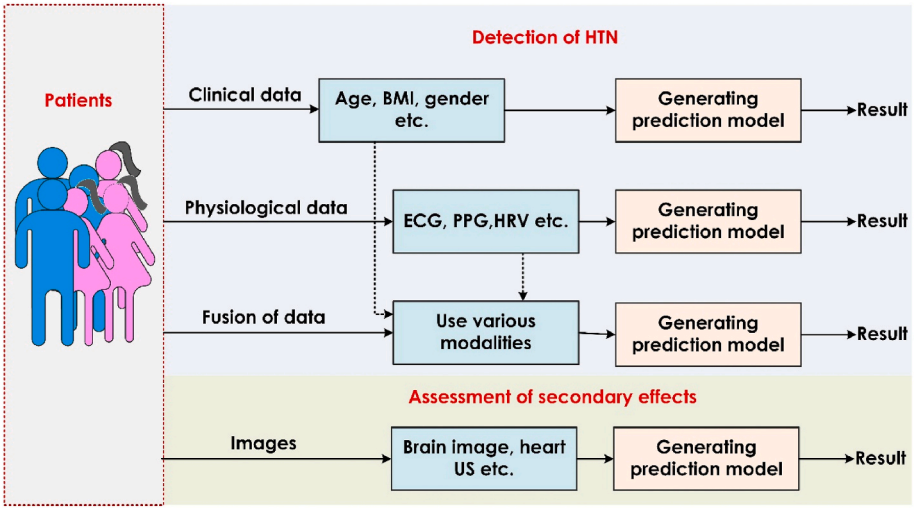

Fig. 3. Illustration of automated detection and assessment of secondary effects of HTN using various clinical, physiological signal and imaging data.

1.4. Contributions

The key contributions of the present review are as follows.

- The systematic review is performed according to the Preferred Reporting Items for Systematic Reviews and Meta-Analyses (PRISMA) [40] guidelines, to establish rigor and transparency.
- The techniques for estimating HTN using all types of data such as clinical, signals, and its secondary effects using imaging modalities are considered for the systematic review.
- The dataset used, feature extraction techniques, ML and Deep Learning (DL) methods, and results of previous related studies leveraging various data modalities.
- The main findings and future research opportunities are discussed.

The rest of the paper is given as follows: Section 2 describes the general procedure followed to perform this review process. Sections 3 and 4 present a detailed review of the AI techniques for HTN prediction and assessment model including all modalities respectively. Section 5 describes the results and discussion with main findings and further research directions. Finally, the conclusion is drawn in Section 6.

2. Search strategy

To promote the transparency and consistency of the review paper, we have followed PRISMA [40] guidelines. The quality of the review paper starts by identifying the articles from the academic database. Further, the process includes identifying the search engine, search string, keywords, and inclusion criteria. The search engines from the academic database such as Scopus, PubMed, IEEE *Xplore*, MDPI, Web of Science (WoS), and Hindawi are considered for this review process. The articles indexed in these databases are deemed to be good quality and reputed. Table 2 shows the various search string or query and inclusion criteria, which is used to collect the relevant papers. In addition, the keywords such as "Machine learning", "Hypertension", "PPG", "ECG", "HRV", "BCG", "Blood pressure", and "Deep learning" have been used to search the articles. The search window frame for the related articles is set to 2013 to 2023, i.e., all the articles published in the last 10 years.

Hence, using search queries a pool of 7280 articles was downloaded from November 3–18, 2023. Finally, based on the inclusion criteria 122 articles were selected as subjects of interest for the current review process. Fig. 4 outlines the article selection process. The articles selected (prior to eliminating the duplicates) from the databases are PubMed at 14.60 %, Scopus at 34.31%, MDPI at 8.03%, IEEE *Xplore* at 10.95%, Hindawi at 5.84 %, and WoS at 36.28%. It is observed that Scopus has the highest number of articles and Hindawi has contributed the lowest number of articles. All these articles are thoroughly reviewed for this study. Table 3 shows the number of articles obtained in various categories for automatic detection and assessment of HTN using search queries from 2010 to 2023.

Table 2
Used search query and inclusion criteria.

Query	Inclusion criteria
• ((Detection) AND (hypertension)) AND (clinical data)) AND (machine learning)) • (detection OR identification) AND (hypertension) AND (cerebrovascular alterations); (computer aided diagnostics) AND (detection OR identification) AND hypertension) AND (cerebrovascular alterations) AND (Brain image) • ((Automatic) OR (detection) OR (identification)) AND ((hypertension) OR (pulmonary hypertension)) AND ((echocardiographic images) OR (echocardiographic measures)) • ((hypertension) AND (retinal fundus)) AND (machine learning); ((hypertension) AND (retinal fundus)) AND (deep learning); ((hypertension) AND (retinal fundus)) AND (artificial intelligence); • (hypertension detection) AND (renal stenosis); (((((hypertension) AND (detection)) OR (identification))) OR (ESTIMATION)) AND (RENAL STENOSIS) • (PPG) AND (Hypertension) OR (Blood pressure) OR (hypertension) AND (machine learning) OR (deep learning) • (ECG) AND (Hypertension) OR (Blood pressure) OR (hypertension) AND (machine learning) OR (deep learning) • (HRV) AND (Hypertension) OR (Blood pressure) OR (hypertension)AND (machine learning) OR (deep learning) • (BCG) AND (Hypertension) OR (Blood pressure) OR (hypertension) AND (machine learning) OR (deep learning)	• The study focuses on the automatic detection of hypertension using machine learning and deep learning. • Articles should be in English and peer-reviewed. • The paper should be available online. • The article should belong to a study on human beings.

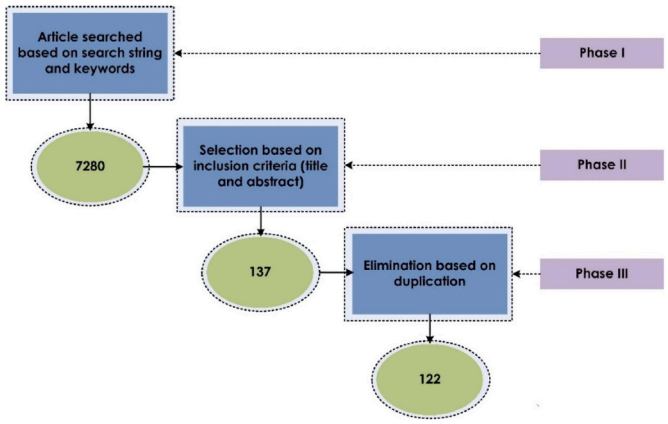

Fig. 4. Process of article selection for this systematic review based on the PRISMA guidelines.

first line of diagnostic test among patients attending cardiology clinics. ECG provides a graphical representation of cardiac rhythm, the direction of resultant electrical impulse transmission, heart rate, and atrial and ventricular activation abnormalities [45,46].

In HTN, ECG is useful in the detection of LVH and arrhythmias. The presence of LVH is related to the severe form of HTN. LVH can be diagnosed using Sokolow Lyon criteria i.e., the amplitude of S in V1+ R in V5 or V6 > 35 mm [47] (Please refer to Fig. 5 (a)).

Photoplethysmography (PPG) Signal

PPG Signal represents arterial and venous blood perfusion. This detects the light reflected from the tissue perfused by the blood vessels using a low-intensity infrared light sensor. The waveform obtained is well correlated with the physiologic data such as heart rate, BP, and blood oxygen saturation [49–51]. The various HTN stages using PPG are shown in Fig. 5(b).

Table 3
Number of articles related to automatic detection and assessment of HTN using search query from 2010 to 2023.

Topics			Sources						Keywords	Total	Duplicate	Final count
			PubMed	Scopus	MDPI	IEEE	Hindawi	WoS				
Clinical data		Total	84	694	387	10	11	63	3	1252	9	**18**
		Relevant	**4**	**11**	**1**	**4**	**2**	**2**	**3**	**27**		
Imaging modality	**Brain**	Total	60	16	14	72	51	7	0	220	0	**6**
		Relevant	**3**	**1**	**0**	**0**	**0**	**2**	**0**	**6**		
	Heart US	Total	485	304	33	125	77	295	0	1319	1	**11**
		Relevant	**4**	**3**	**0**	**0**	**1**	**4**	**0**	**12**		
	Retinal	Total	86	386	113	8	13	816	0	1422	4	**6**
		Relevant	**1**	**5**	**1**	**1**	**0**	**3**	**0**	**11**		
	Kidney	Total	1070	56	151	19	92	1314	0	2702	0	**2**
		Relevant	**0**	**0**	**0**	**0**	**0**	**0**	**2**	**2**		
Signal modality	**PPG**	Total	6	38	13	18	6	39	1	121	0	**39**
		Relevant	**2**	**12**	**5**	**6**	**3**	**13**	**1**	**42**	0	
	ECG	Total	6	22	4	0	4	17	2	55	0	**24**
		Relevant	**3**	**11**	**1**	**0**	**0**	**9**	**1**	**25**	0	
	HRV	Total	3	6	3	6	3	4	0	25	0	**9**
		Relevant	**1**	**3**	**1**	**3**	**2**	**1**	**0**	**11**	0	
	BCG	Total	4	3	4	3	2	4	0	20	0	**7**
		Relevant	**2**	**1**	**2**	**1**	**0**	**2**	**0**	**8**	0	
		Total	**1824**	**1572**	**733**	**276**	**267**	**2595**	**13**	**7280**	**14**	**122**

3. Detection of HTN

The complete analysis of the detection of HTN is described in this section.

3.1. Using clinical data and physiological signals

HTN can be diagnosed using various approaches in medical centers such as i) using clinical data, and ii) using physiological signals. The detailed description is explained in the subsequent section.

3.1.1. Clinical data

There are several risk factors for HTN such as age, obesity, high intake of dietary salt, smoking, alcohol consumption, tobacco use, sedentary lifestyle, diabetes mellitus, abnormal lipid profiles, etc. [41–43]. Few of these exhibit major predisposing factors for the development of young HTN [44]. Certain modifiable risk factors have been demonstrated to be the major concern in management.

3.1.2. Physiological signals

Electrocardiography (ECG) Signals

An ECG depicts the electrical activity of the heart and is used as the

Heart Rate Variability (HRV) Signal

HRV analysis demonstrates the temporal changes in the heart rate i.e., R–R interval from beat to beat. These are traditionally assessed using ECG signals and are used in clinical and functional cardiac assessment. The HRV depicts autonomic neuro-regulation of the sequential heart rate [52]. Altered autonomic nervous system regulation and decreased HRV have been demonstrated in the development of HTN [53–55].

Ballistocardiogram (BCG) Signal

BCG technique is used to record the micro-vibration of whole-body recoil forces resulting from displacement, velocity, and acceleration of the blood flow when the heart pumps out the blood with each beat. Hence this reading also resembles the physiologic heart data [56–59]. This can detect temporal changes in BP, stroke volume, and pulse transit time during rest and exercise. Thus far this also can be used to monitor HTN. Particularly acute rise in BP during exercise marks the risk factor for the development of HTN and overall cardiovascular events [60,61]. An example of BCG signals is shown[2] in Fig. 5 (c).

[2] https://doi.org/10.6084/m9.figshare.7594433

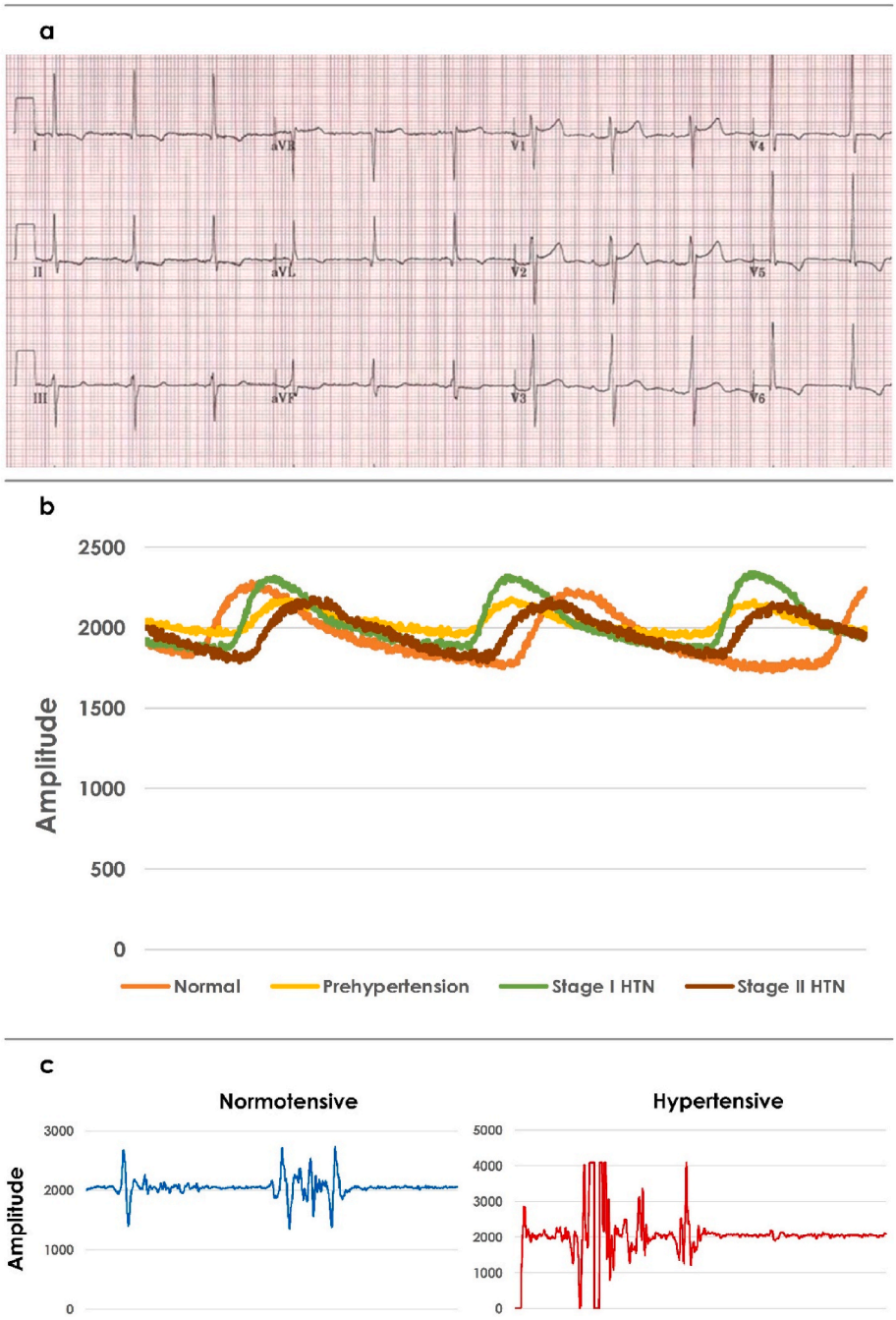

Fig. 5. Examples of signal processing approaches used in the past work for automated HTN detection. a) LVH detection using ECG, b) Comparison of various stages of HTN using PPG signals [48], and c) Illustration of BCG signal with initial 2000 samples.

3.2. Detection of HTN using CAD tools: datasets, features, classifications, and techniques

Many researchers have used clinical data and physiological signals to identify HTN automatically. A details description of these methods is explained in the below section.

3.2.1. Clinical data processing

Recently many clinical/medical attributes have been used to identify whether the person is having HTN or not. The patients' detailed clinical information is publicly available in the Multiparameter Intelligent Monitoring in Intensive Care II (MIMIC-II) database [62]. Along with the waveforms, it also includes typical numerals such as heart rate, SpO2, DBP, and SBP, etc. To track hypertensive patients many surveys and data collection have been carried out such as National Health and Nutrition Examination Survey (NHANES) on the U.S population [63], Korean National Health Insurance Corporation (NHIC) [64], and Canadian Primary Care Sentinel Surveillance Network (CPCSSN) [65]. Many researchers have utilized these datasets to build classification models. In addition, authors have also used private datasets to predict HTN.

Generally, many ML techniques such as K-Nearest Neighbour (KNN), Naive Bayes (NB), SVM, RF, logistic regression (LR), multi-Layer Perceptron (MLP), Decision Tree (DT), Extreme Gradient Boosting (XGB) are utilized to predict HTN using physiological parameters [34,35,66–68]. The physiological parameters such as age, gender, BMI, BP, heart rate, cholesterol etc., are used commonly to show the best prediction of HTN. Some works have used 3 [69], 4 [34,70], 8 [35,66], and 11 [71] features or clinical attributes to achieve better outcomes.

Moreover, in Ref. [66] Convolutional Neural Network (CNN) is developed, which achieved better efficacy when compared to other classification techniques such as KNN, RF, and NB. To select the proper risk factors or features, the authors have used the Boruta-based feature selection approach [68]. Further, to avoid the imbalance class problem Adaptive Synthetic (ADASYN) was utilized [68,72]. In Ref. [73] Synthetic Minority Oversampling Technique (SMOTE) was used to generate the synthetic data of the minority class.

In addition, to enhance the efficiency of the model hybrid model is generated by combining KNN and Light Gradient Boosting Machine (LightGBM) [74] and Bidirectional Long Short-Term Memory (BiLSTM) and autoencoder networks [75]. Since disease symptoms in terms of textual sentences also key information, that is embedded in the layer [75].

Further, SHapley Additive exPlanations (SHAP) are used to visualise the risk factors based on Shapley values, which explains the contribution of risk factors while predicting HTN using ML approaches [68,76,77]. The method XGB with SHAP analysis shows that weight, age, income, fat, diabetes mellitus, BMI, history of HTN, salt, smoking, and drinking were the related risk factors for developing HTN [68]. Table A1 shows the summary of the ML-based methods using clinical data/parameters.

3.2.2. Public dataset for signal processing approaches

MIMIC (Medical Information Mart for Intensive Care) is a large, freely available database comprising de-identified health data associated with over 40,000 critical care patients. It includes data from demographics, vital signs, laboratory tests, medications, etc. from ICU stays at Beth Israel Deaconess Medical Center. A few of its variants include.

MIMIC-II [78] (v2.6): Released in 2012, containing data from 2001 to 2008.
MIMIC-III [79] (v1.4): Released in 2016, containing data from 2001 to 2012 with improved data integration over MIMIC-II.
MIMIC-IV [80]: Released in 2023, containing data from 2012 onward.
eICU Collaborative Research Database [81]: Multi-center ICU database complementing MIMIC, released in 2018.
MIMIC-Extract: A subset of 12,000 patients from MIMIC-III prepared to facilitate machine learning.
MIMIC-Waveform Database [82]: Subset of MIMIC-III with matched waveforms (ECG, PPG, etc.) for over 30000 patients.

Key benefits of MIMIC include the large sample size, breadth of variables, and public accessibility, enabling many analyses and ML applications. Limitations include a restricted patient population, potential inaccuracies in some measurements, and the need to apply for access. Overall, MIMIC has proven invaluable for critical care research.

In addition, SHAREE [83] (Smart Health for Assessing the Risk of Events via ECG) is a large dataset focused on ECG data and CVD risk stratification. The database contains over 10,000 ECG recordings from 139 subjects along with demographic data, lab tests, medical history, etc. It includes healthy subjects as well as those with risk factors or established cardiac disease. ECGs were obtained using a 12-lead, 10-s, 500 Hz sampling rate. The database consists of three sets of data: SHAREE Set 1 consists of - 1000 healthy subjects data which were used to establish the normal ECG ranges; SHAREE Set 2 was obtained from the remaining subjects with cardiac risk factors or disease; and SHAREE GOLD which is a subset of Set 2 with expert annotations of abnormalities.

The database has been used in developing ECG-based models for detecting cardiovascular risk factors and disease, as well as in the training of DL algorithms for ECG interpretation. The limitations of the database include a small diversity of the population (data were obtained from a single collection site only), and no continuous ECG or other waveform data beyond 10-s 12-lead ECGs.

3.2.3. Approaches using PPG

The process of collecting high-fidelity PPG signals starts with appropriate sensor selection and placement considering variation across demographics. Calibration procedures adapt illumination wavelength and intensity to optimize the reflected signals for a particular skin type and measurement site. The analog signals are digitized through precise ADC modules to avoid quantization noise and errors. Understanding the hardware subtleties enables the acquisition of pristine signals before they get contaminated through interactions with physiological processes.[3]

In our review of existing literature, we noted that a predominant focus of prior investigations in this application domain is extensive exploration of methods for optimal feature selection and extraction. The vast majority of studies dedicate substantial efforts towards engineering discriminating representations from the raw data pruning non-informative attributes. This indicates that specialized feature curation through transformation techniques [84–97] such as Synchrosqueezing Transform (SST) used in Ref. [84] is a time-frequency analysis technique that can provide a sharper representation of the instantaneous frequencies within a signal, Tunable Q-factor Wavelet Transform (TQWT) used in Ref. [98] enables changing the frequency resolution levels dynamically during signal decomposition and processing by altering Q-factor values, and Principal Component Analysis (PCA) is employed in Ref. [99] transforms the data into fewer dimensions which are a linear combination of the original features while retaining as much information as possible, Linear Discriminant Analysis (LDA) employed in Ref. [100], which projects high-dimensional data onto a lower-dimensional space such that the classes are well-separated and variance between members of the same class is minimized.

The informative numerical representations extracted from the pre-processed signals are leveraged to develop automated classification models using ML algorithms. A study [100], employed RFs which work by aggregating predictions from an ensemble of DTs trained on random subsets of features to boost accuracy and control overfitting. SVMs as shown in the study [97] identify optimal hyperplanes to maximize separation between classes using kernel functions to project features to higher dimensions and study [96] where K-Nearest Neighbors have been used to categorize instances by plurality votes of the K most similar labelled examples in the feature space through distance metrics.

ANN, with multilayer architectures of interconnected neurons, performs robust pattern recognition via hierarchical feature transformations and nonlinear activations. These are very popular amongst research as these can approximate complex non-linear functions, studies [101,102] have employed and achieved profound results. DL approaches like CNN and Recurrent Networks take this automated feature learning to advanced levels with deeper abstractions. While classical ML relies on engineering the features, deep networks can operate directly on the raw signal inputs and optimize their complex feature hierarchies tailored to the problem through end-to-end training. Combining extracted domain features with learned representations has also shown promise. Table A2 summaries all the models employed and their corresponding results.

3.2.4. Approaches using ECG

Acquisition of high-fidelity ECG recordings requires careful consideration of the type and placement of leads to capture all significant cardiac activity information. Multiple leads are used to provide different perspectives across the 3D volumetric spatial field around the heart. The signals should have minimal noise or motion artefacts with at least 200 samples per second to discern key components like the P wave, QRS complex, and T wave for analysis. Signal fidelity impacts what can be extracted downstream so quality recording procedures and calibrated sensors are crucial [103].

[3] (PPG_sig_proc_Chapter_20210612.pdf (peterhcharlton.github.io)).

The time-series ECG signals can then be analyzed in the frequency, time, and time-frequency domains and through nonlinear methods [104] to extract discriminative features. The Fourier Decomposition Method (FDM) [105] leverages the Fourier Transform's ability to capture the constituent sinusoidal components contained within signals to break down and examine their fundamental frequency characteristics. Time-frequency distributions like the Wigner-Ville distribution provide joint spectro-temporal views. Wavelet Transforms [106,107] extract multi-resolution characteristics effectively via dilation and translation operations on a mother wavelet. Statistical features like kurtosis, entropy and higher-order moments also contain relevant discriminatory information.

For classification, these engineered inputs from standard ECG segments can train ML models like RFs [108] and SVMs [109] to categorize arrhythmias. Deep Neural Networks (DNNs) [110–118] and Recurrent Architectures [119,120] can operate directly on raw ECG signals to learn hierarchical representations suited for the classification task in an end-to-end fashion without relying on hand-crafted features through sufficient training data. Attention mechanisms are also being explored to selectively focus on informative sub-components automated ECG analysis. Table A3 summarizes all the studies with ECG Signal as the basic modality.

3.2.5. Approaches using HRV

HRV data acquisition involves capturing the time intervals between consecutive heartbeats, reflecting the autonomic nervous system's activity. This data is collected through ECG recordings or wearable devices. Signal processing techniques are applied to extract features from this data for analysis. Statistical analysis [107,121], is seen to be the prime feature extraction and analysis technique and to quantify the variability in heart rate intervals, offering insights into an individual's physiological state.

Moving beyond basic statistical measures, non-linear frequency feature components play a pivotal role in HRV analysis. Metrics like time and frequency domain measures [56,122–125] and non-linear measures [122] capture the complexity and irregularities in the heart rate dynamics, providing a more comprehensive understanding of the cardiac system's behaviour.

Wavelet transform [126] stands out as a powerful tool for HRV analysis due to its ability to capture both frequency and time-domain information. It breaks down HRV signals into different frequency components, allowing for a detailed exploration of transient changes and abrupt variations in heart rate dynamics across different scales. This approach facilitates the identification of subtle patterns that might not be evident in traditional signal-processing methods.

Once relevant features are extracted, ML models such as KNN and SVMs [122,123,125] come into play for classification tasks. These models leverage the extracted features to differentiate between various physiological states or pathologies. KNN, based on similarity measures, classifies new data points by comparing them to their neighboring points in the feature space. SVM, on the other hand, seeks to find an optimal hyperplane to separate various classes in the feature space in best possible way.

Integrating these methodologies—data acquisition, statistical analysis for feature extraction, utilization of non-linear frequency components via wavelet transforms, and application of ML models—forms a comprehensive framework for understanding HRV patterns and their implications for health monitoring and clinical diagnosis. This multi-step approach enhances our ability to decipher the complexities within HRV data and contributes significantly to the field of physiological signal analysis. Table A4 summarizes the results and methodologies of studies using HRV as a modality.

3.2.6. Approaches using BCG signals

BCG is a non-invasive method used to evaluate cardiac function by measuring the body's subtle movements in response to the heart's ejection of blood with each heartbeat. Originally conducted on specialized beds or platforms, modern BCG employs advanced sensors or devices to capture these minute body motions, providing insights into cardiac performance and assisting in the assessment of heart function based on the generated movements throughout the cardiac cycle. Similar to HRV analysis, statistical analysis [127,128] is employed for feature extraction from BCG signals. Parameters such as mean, standard deviation, and variance aid in characterizing the dynamic changes in blood flow and volume. These statistical measures offer insights into the cardiac cycle and cardiovascular health, providing valuable markers for analysis and interpretation. Non-linear frequency feature components play a significant role in BCG signal analysis, capturing the complexities of cardiac dynamics beyond basic statistical measures.

Wavelet transform [129–131] serves as an effective tool in BCG signal processing, allowing the decomposition of signals into different frequency components across time. This technique enables the analysis of transient changes and variations in blood flow dynamics at various scales, aiding in the detection of subtle patterns and anomalies that might not be apparent through traditional signal processing methods.

For classification tasks in BCG-based analysis, ML models like KNN and ANN are utilized. These models leverage extracted features to classify different physiological states or abnormalities. KNN identifies similar patterns by comparing data points' proximity in the feature space. DNNs have emerged as a powerful tool in the analysis of BCG signals due to their ability to learn intricate patterns and representations directly from raw data. When applied to BCG-based data, DNNs can autonomously extract hierarchical features, bypassing the need for handcrafted feature engineering. With their multiple layers of interconnected nodes, DNNs can uncover complex relationships within BCG signals, capturing nuanced variations and subtle irregularities that might elude traditional feature extraction methods. Techniques like CNNs [132] can efficiently process temporal data, while recurrent neural networks (RNNs) excel in handling sequential information within BCG signals. The integration of DNNs into the analysis pipeline complements existing methodologies, enhancing the accuracy and depth of insights gleaned from BCG data, thus contributing to more precise diagnostics and a deeper understanding of cardiovascular health. Table A5 summarizes the results and methodologies of studies using BCG as a modality.

3.2.7. Approaches using fused data processing

In the realm of biomedical research, the convergence of various physiological data streams has sparked immense curiosity, yet only a scant few studies have delved into the fusion of modalities, specifically integrating PPG, ECG, HRV, and BCG data. Studies are also performed by combining the various imaging modalities such as Echocardiography, CT, X-rays, and MRI as well as combining imaging modality with clinical indicators or with signals. The studies were also conducted for the diagnosis of Hypertensive Heart Disease (HHD) and Hypertrophic Cardiomyopathy (HCM) by combining echocardiography and electrocardiogram (ECG) [133]. The authors have used CNN [134], Shallow Neural Network [102], LSTM [119,135], CNN-LSTM network [120,136], ResNet [137] to achieve better performance wherein PPG and other modalities (such as arterial blood pressure (ABP) and ECG) are combined. The studies were conducted with the combination of echocardiographic measures and Chest X-rays for classifying Pulmonary Hypertension (PH) and healthy subjects with various DL approaches such as Xception, Inception V3, and ResNet50 [138]. It is also noted that frequency domain features [56,127,139,140] are used with HRV in combination with other modules to perform remarkable results. The study has used univariate logistic analysis and the Gini impure technique for feature selection [36]. Further to reduce the complexity and to highlight the significant features, feature selection techniques such as Fisher's discriminant ratio (FDR), information gain, and Relief-F algorithms were also employed [133]. Studies have used ML-based classifiers such as SVM [133], MLP, and RF [37] for classification.

For the dataset, studies have collected data from various sources. From the retrospective analysis, 200 patients with HTN were collected by Ref. [141], and 7532 patients' data was collected by Ref. [36] which consists of demographic information, comorbidities etc., along with CT reports. A study has also collected data from mobile wearable smart devices related to walking, work and exercise along with ECG data [37]. Studies have used SMOTE for balancing the dataset [36]. These pioneering investigations, albeit limited in number, have yielded remarkable and profound outcomes. Table A6 summarizes the studies with the fusion of modality with the results.

4. Assessment of secondary effects of HTN

The various imaging modalities and CAD tools are described in this section.

4.1. Imaging modalities

HTN cannot be diagnosed by various imaging modalities such as MRI, US, fundus imaging, etc. This imaging represents the secondary changes due to long-standing HTN. The detailed description of the imaging modalities is explained in the below section.

4.1.1. Brain images

Population-based MRI studies have demonstrated white matter lesions in the brain among individuals with high BP recordings [142]. The severity of white matter lesions in MRI was well correlated with the severity of HTN [143]. These cerebral changes were also associated with an increased risk of stroke, dementia, and cognitive decline [144–146]. Fig. 6 (a) shows the sample hypertensive brain image.

4.1.2. Heart ultrasound images

Echocardiography is a widely used noninvasive diagnostic test that evaluates cardiac structure and function. In HTN, echocardiography describes the Left Ventricular (LV) geometry and mass that defines LVH and the type of LV remodeling. Follow-up echocardiographic assessment is advised to evaluate the regression of LVH to check the response to anti-hypertensive therapy [147,148]. Echocardiographic measurement of LV mass and detection of LVH require good image quality and accurate measurement of the hinge points of the ventricular walls. The use of AI has shown promising results in accurate measurements of cardiac structural and functional changes [149]. In addition, two-dimensional echocardiographic imaging can readily display chamber dimensions, left atrium and left ventricular volumes, and aortic root size [150] Further Echocardiography is also useful in the evaluation of LV diastolic dysfunction, often impaired in HTN patients even in the absence of LVH [151]. In HTN generally, LV remodeling takes place in a concentric manner, with an increase in LV mass and relative wall thickness [150]. Echocardiographically demonstrated LVH and other cardiac structural and functional alterations possess increased CVD risk [152,153]. LVH due to HTN exhibits LV thickness of more than 12 mm with a relative wall thickness > 0.44 suggesting concentric remodeling. Also, left atrial size and volume are elevated proportionately with the elevated diastolic dysfunction grade among HTN patients (please refer to Fig. 6 (b)).

4.1.3. Retinal images

Diagnosis of Hypertensive Retinopathy (HRT) and its severity can be made using retinal fundoscopic imaging. Severe forms of retinal damage predict all-cause mortality in HTN patients and are often used in risk stratification [154,155]. Other forms of hypertensive-related retinal damage may exhibit retinal hemorrhage, cotton wool spots and microaneurysms [156]. Some sample fundus images are shown in Fig. 6 (c).

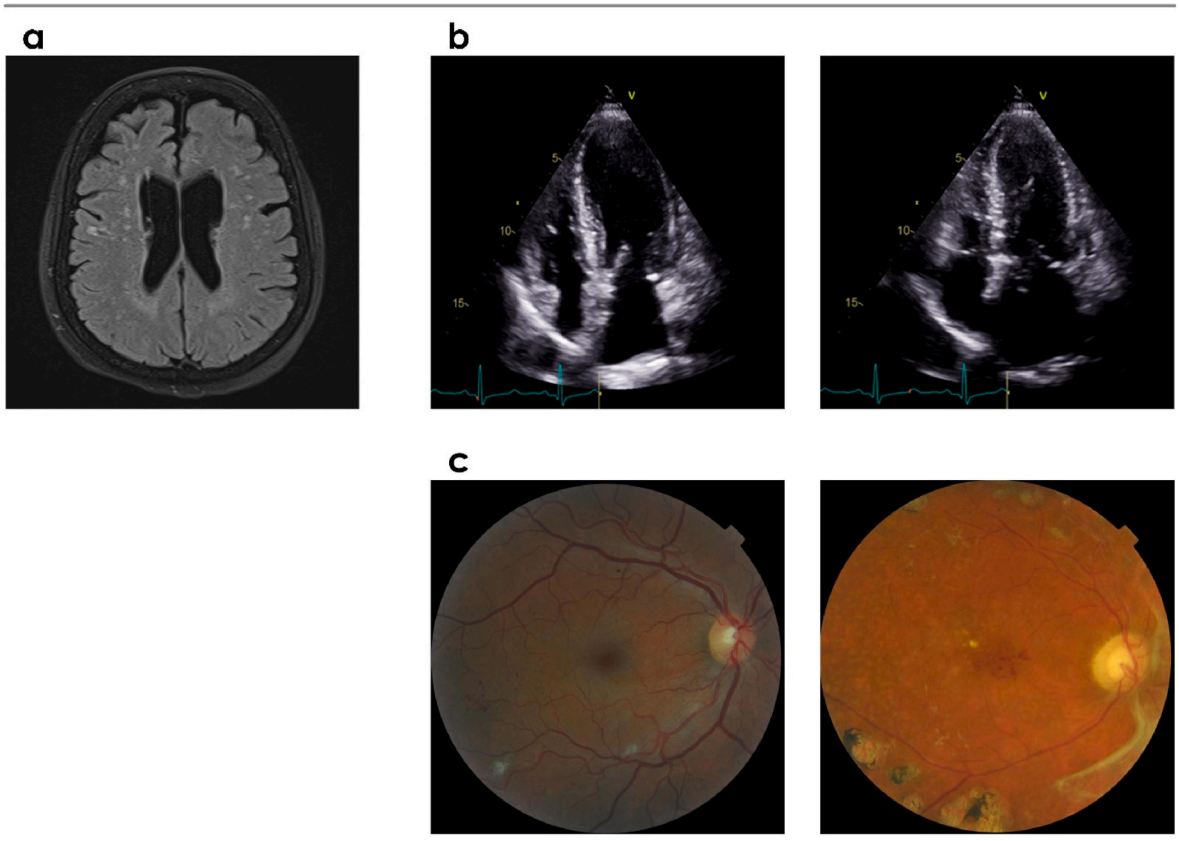

Fig. 6. Sample hypertensive patient images captured through various imaging modalities. A) T2 Flair hyperintensities noted in a patient with HTN, b) Apical 4 chamber view at end-diastole and end-systole, and c) HTN fundus images.

4.1.4. Kidney images

US imaging of the kidney depicts the size and structure of the kidney and helps in identifying reno-vascular disease and renal artery stenosis if present [31]. Spectral Doppler application in kidney US also assesses renal resistive index which is a marker of atherosclerosis and HMOD [32].

4.2. Assessment of secondary effects of HTN using CAD tools: datasets, features, classifications, and techniques

4.2.1. Using brain images

The human brain starts to show a modification in its structure much earlier than the beginning of HTN. Studies also have shown that there exists a relationship between the changes that occur in the diameter of the blood vessel and HTN development. These changes in the cerebral vascular lead to an imbalance in blood circulation to the brain. A study [157] also suggests that the reason for HTN may be to sustain a balance in blood flow to the brain [38]. Follow-up on tortuosity and diameter modification of vessels helps in the evolution of HTN [158]. By using MRA imaging these structures can be very well visualized [159]. MRA imaging can track these changes. However, the key stage in this process is to segment the cerebral vasculature from the complex human brain structure. The automatic segmentation of vascular structures and then the quantification of the modification in diameter and tortuosity could be very-helpful to clinicians in early diagnosis. This can be well achieved with the help of CAD tools. The researchers have proposed several studies to segment and then predict the presence of HTN.

Datasets are one of the major concerns in generalizing the developed model. Most of the studies have tested their model based on a personal dataset developed. The subjects considered for the study were in the range of 15–342 subjects. MRA imaging of the patients was collected using a 3T Trio TIM scanner [160,161], which produced 3D images. The subject's BP was also measured with the help of a sphygmomanometer twice with a minimum gap of 1 min between each measurement [160].

Segmenting the region of interest is one of the major steps in medical image analysis. Segmenting of the cerebral blood vessels is quite challenging because of the noise induced during the MRA image acquisition process, the complex structure of vasculature, small diameter vessels, etc. Usually, a pre-processing stage is involved as a base for segmentation. While capturing the brain images using MRA, commonly, the intensity of images was non-uniform. A bias correction algorithm was used to correct these non-uniformities [160,162]. Further, the non-homogeneities were reduced using a 3-D Generalized Gauss-Markov Random Field (GGMRF) model [38,160,162] and 3D Rotational and Translational Invariant GGMRF models [161] were used. Segmentation was either performed by using a 3-D Local adaptive segmentation algorithm [162] or by using 3D –CNN [38,160].

The major feature for detecting the presence of HTN is modification of the blood vessel in terms of its diameter and tortuosity. Hence, the final segmented blood vessels were further analyzed to detect the modifications present in termers of diameter and tortuosity. Studies have found Median vascular radius [162], vessel diameters [38,160] and tortuosity [38,160,162,163]. Blood vessel diameters were extracted using a distance map [160,162] and tortuosity was identified using mean and Gaussian curvatures [38,160,162] of the brain.

Further, the classification between normal/prehypertensive, and hypertensive was done either by using ML techniques or by using DL models. Studies have used ML models such as SVM [160], ensemble bagged trees, ensemble RUSBoosted, ensemble Subspace KNN, and KNN [158]. Studies have also used ANNs and achieved remarkable results [38]. Table A7 summarizes the various studies performed using MRA images for the detection of HTN.

4.2.2. Using heart ultrasound images

The increased level of the mean pulmonary arterial pressure (PAP) when measured during the rest state is termed PH. This disorder may lead to many clinical-related complications. It can affect respiratory as well as cardiovascular-related disorders. This may also lead to death if this condition is not treated timely. Right heart catheterization measures the pressure directly hence it is considered as one of the well-known methods to obtain the quantitative value of PAP. This is an invasive kind of test and involves minimum risk [138]. Non-invasive methods like US of the cardiogram are also used to determine the presence of HTN with its detection rate being around 73.15%. This non-invasive technique has gained popularity in the clinical assessment of HTN. It can identify the increase in the blood vessels by using US waves [164]. Many of the studies are using only cardiac US images also known as echocardiography for assessments of PH [39,165–170].

Researchers have used private datasets developed for HTN detection with a range of subjects varying from 49 to 346. Some are retrospective studies based on the data collected from various hospitals [166]. Echocardiographic examination was performed in various systems some of them being the Vivid GE healthcare system [39,165], GE Logic S8 [168], and Philips ultrasonic machine [170]. The labels and other unwanted areas were removed from the image by using a masking technique and further, the image's intensities were adjusted using histogram equalization techniques [39,168].

Features are extracted from these pre-processed images by using a Global Weighted Local Binary Pattern (GWLBP) [165]. A study has also used various transformation techniques to enhance the significant details. The study has combined it with the Locality-Sensitive Discriminant Analysis (LSDA) feature reduction technique and observed that Continual Wavelet Transform and Discrete Wavelet Transform (DWT) overfitted the data. Whereas Shearlet Transform and Contourlet Transform have produced better performance [39]. Also, a study has ranked the features using the student t-test [165].

Some investigators have used various DL approaches such as Xception, Inception V3, and ResNet50 [138], 2D-CNN [167,171], spatio-temporal convolutional architectures with ResNet18 as a base model [168] and 3D ConvNet feature extractor [169]. Moreover, studies have used ML-based techniques for the prediction of PH [166,170]. SVM classifier is used in multiple studies [39,133,165,166] along with other classifiers such as RF [166], DTs [39], etc. Table A8 summarizes related work that predicts HTN using heart images.

4.2.3. Using retinal fundus image

The primary measures of fasting glucose level, BP level etc., can define the presence of disorders like hyperglycemia and HTN respectively. Most commonly these diseases are seen with one another, and they also cause the risk of CVD. Worldwide this is observed as the major cause of morbidity and mortality [172]. Population growth, physical inactivity, and the rise in obesity are the major contributors to these diseases [173]. Imaging of the retinal fundus is one of the non-invasive expeditious ways for detecting microcirculatory modifications caused by chronic diseases before they lead to more complications. Owing to the advancement of digital imaging techniques, the retinal photo captured by a fundus camera or by scanning laser ophthalmoscope provides details of the minute changes in the blood vessels of the retina [172]. However, it may be cumbersome for ophthalmologists to manually assess the presence of these disorders in the large, affected population. Using CAD tools quantitative characteristics such as blood volume thickness of vascular caliber can be extracted from these images automatically thus helping in early identification of these disorders. The alterations in blood vessels could be due to an increase in BP or HTN. For persons undergoing regular examination of the eye, this retinal imaging can give a hint of the presence of HTN at a very early stage [174].

There are publicly available datasets for the prediction of HTN from the retinal fundus images. DRIVE dataset [175] is a publicly available database with 40 images. It consists of both original images and

manually segmented images by two specialists. Northern Ireland Cohort for the Longitudinal Study of Ageing (NICOLA)[4] is another dataset that is available on request. It has data from 460 participants; however, the 20 participants' retinal images were obscured. Based on the measurement of clinical BP 151 subjects were classified as hypertensive [174]. DR HAGIS is another publicly available database[5] where images 11 to 20 belong to the HTN subgroup [176]. DIARETDB0 [177] and DIARETDB1 [178] are other databases that could be used for the detection of HTN from retinal images. Studies have also used private datasets which consists of 650 non-HTN subject images and 650 HTN subject images [179].

The images collected from the database are subjected to a pre-processing technique to extract the region of interest. To acquire the optic disk, mathematical morphological operations are performed. For vessel detection monochrome images are preferred as they enhance the visibility [173]. However, by this conversion, useful information might get lost. Hence a study has used the CIEL*A*B* color space model to create images that are more uniform for human perception of colors [179]. Fuzzy logic techniques are also used to improve the brightness [180]. Studies have also used DL-based models derived from Inception-v3 [172], ResNet-152 [180], transfer learning (TL)-based MobileNet architecture [181], and a combination of a deep residual learning network for training the features and DenseHyper a multilayer CNN model [179]. A study has also used a supervised ML classifier [174]. Table A9 summarizes the prediction models for HTN using retinal fundus images.

4.2.4. Using kidney images

Unlike primary HTN, secondary HTN has a known cause. Renovascular stenosis, vascular and endocrinologic diseases, and renal parenchymal disease are common causes of secondary HTN. Renal ischemia from renal artery stenosis leads to renovascular hypertension [182]. For the disorders related to adrenal glands and renal parenchyma, imaging techniques such as CT, MRI, or ultrasonography can be made use of. Vascular disorders and renovascular stenosis could be best identified by conventional or non-invasive (CT or MR) angiography or by using Doppler US. For the endocrine-related causes nuclear imaging could be used [141]. There are clinical studies related to the prediction of HTN from renal artery stenosis, but the studies with the application of CAD tools for the prediction of HTN it limited. CAD tool-based studies have combined imaging of the kidney with other clinical indicators for the prediction of HTN. Herein, we have combined the studies with multi-modality under the Fusion data category.

5. Result and discussions

This paper reviews HTN detection approaches as follows (% of articles used): clinical data processing (13.93%), signal processing (51.64%), and fused data processing (18.03%). Image processing (16.39%) approaches evaluate the structural changes of human organs. Fig. 7 shows the distribution of these articles across the years. However, researchers have more recently begun exploring image-based approaches, likely seeking to identify optimal ML algorithms for integrating diverse data types. The majority of work involved signal processing using modalities like ECG and PPG. While clinical data studies were less common, fused and imaging approaches have grown in recent years, indicating an effort to develop more comprehensive models leveraging different data sources. This distribution highlights past focus areas and evolving priorities around multi-modal integration for HTN detection.

From Table A1-A9, it is observed that ML and DL techniques are fairly used in the various detection approaches. However, some statistical methods are also used in image and fused data processing approaches. Fig. 8 illustrates the summary of the distribution of various strategies used in the detection of HTN. This confirms that ML-based techniques are often employed in the automated identification of HTN, specifically used in clinical and signal processing approaches.

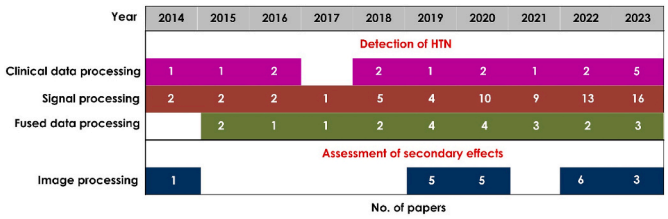

Fig. 7. Number of papers published on automated HTN detection from 2014 to 2023. Papers are categorized based on their primary scope, distinguishing between HTN detection and assessment of secondary effects, as well as the type of data utilized, further classified into clinical, signal, or image datasets.

Generally, CAD tools developed using these methods are evaluated by using accuracy, specificity, precision, sensitivity, and F1-score generated from the confusion matrix [183]. It is observed that many CAD tools in various fields have applied the same performance measures [184–189]. The F1-score is computed using recall and precision values and it can be used to further compare the performance of various models [18]. In addition, another important performance parameter is the area under the receiver operating characteristic curve (AUC), which acts as a key indicator for continuous changes between the true and false positive rates. The range of AUC is from 0 to 1, i.e., 1 means the classifier properly classifies the classes and 0 means wrong prediction [190]. The performances of each approach are described in the following section.

5.1. Detection of HTN

Although HTN is diagnosed when BP readings show a higher range, clinically these patients may exhibit certain signs and symptoms that raise the suspicion of HTN. For instance, dizziness, headache, fatigue, etc., primarily become warnings for checking the BP in the adult population [4, 8]. Certain clinical data such as age, gender, BMI, family history, smoking history, etc. are used in the development of a predictive model for new onset HTN. However, a significant proportion of HTN patients remain asymptomatic, presenting only with advanced disease pathology or end-organ damage. Additionally, some individuals have fluctuating BP readings that complicate timely diagnosis and management. Given these challenges, physiological signals like pulse wave velocity, PPG, BCG, and ECG are often used for HTN prediction and diagnosis [45–49].

5.1.1. Clinical data processing

It is observed from Table A1 that the various physiological factors can classify the subjects into normal and HTN using ML models efficiently. In Ref. [191], Gradient Boosting Machines (GBM), LDA, XGB, and LR exhibit the highest accuracy of 90%. All GBM, XGB, LDA, and LR are achieved F1-score of 95 % and a recall rate of 100%, which comparatively better when compared to other techniques. The ML models showed that BMI and age are significant factors for HTN [191]. Among all various classifiers, RF achieved an AUC of 0.816, though the sensitivity is comparatively less when compared to XGB [67]. Interestingly, it is also noted that RF performs better than medical protocols [67]. It is also observed that LR showed a better accuracy of 82.9% when compared to DT, RF, and Gradient Boosting (GB) models [192]. However, KNN also showed better performance by achieving a maximum accuracy of 86% [74]. In Ref. [35], only eight features are exploited to obtain the system accuracy of 99.5% using C4.5 DT and RF classifier. The authors have also used a 5-fold cross-validation scheme to avoid the biasing. Moreover, the C4.5 DT and RF classifier obtained an AUC of 1

[4] https://www.qub.ac.uk/sites/NICOLA/InformationforResearchers/.
[5] https://personalpages.manchester.ac.uk/staff/niall.p.mcloughlin/.

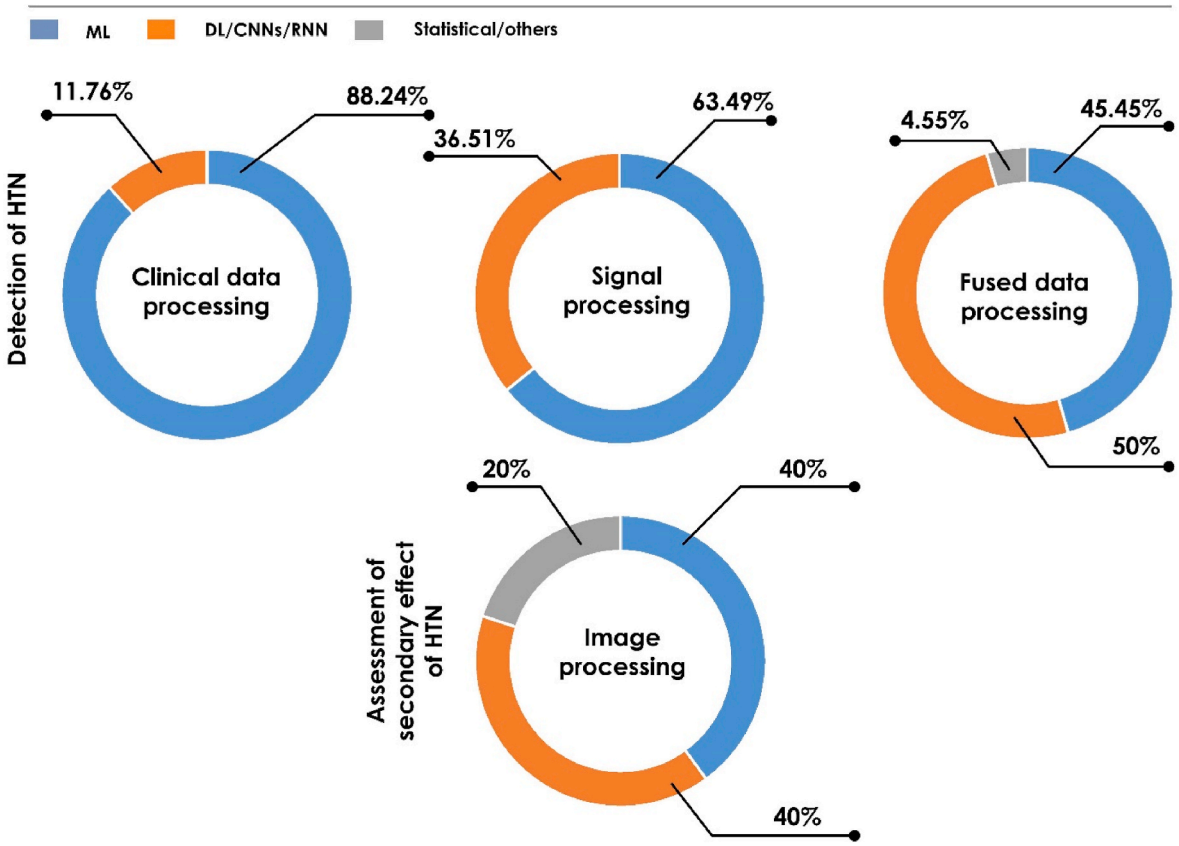

Fig. 8. Summary of the various techniques used for the automated detection of HTN. The papers are categorized by the main task (hypertension detection vs assessment of secondary effects) and the type of data used (clinical data, physiological signals, medical images). Within each category, the methods are further divided into machine learning (ML), deep learning (DL), and statistical techniques.

for normal, pre-HTN, and stage-2 HTN and 0.99 for stage-1 HTN. In Ref. [66], CNN showed better performance by achieving an accuracy of 89.95%, when compared to other ML methods such as KNN, RF, NB, etc. and used *eight* features. It also noted that the authors have used BiLSTM and autoencoder to learn textual description and physical indicators respectively from EHR [75]. They achieved an accuracy of 89.7% and hence extracted the full information from EHR. In Ref. [193], 4 measurement types such as glucose, BP, weight, and BMI are considered and obtained an accuracy of 90% using a neural network model. Recently the model based on the XGB [68] has achieved an accuracy and AUC of 88.81% and 0.894, respectively. It also achieved the F1-score of 93.18% and recall of 97.04%. It observed that age, weight, and fat are the 1st, 2nd, and 3rd leading causes of HTN. SHAP analysis has also shown that these factors are significant risk factors associated with the occurrence of HTN [68]. Fig. 9 shows the performance of various techniques used in the prediction of HTN.

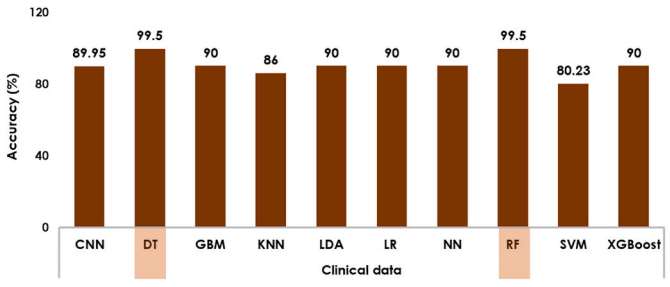

Fig. 9. Summary of maximum accuracy(%) obtained using clinical data for automated hypertension detection with various machine learning techniques. Studies utilizing DT and RF classifiers achieved maximum accuracy.

Existing systems have limitations. They rely on potential risk factors collected from specific demographic populations through cross-sectional studies. It is difficult to generalize such systems, as numerical risk values may change over time. Additionally, different ML algorithms produce varying prediction rates, making it challenging to determine the most suitable model. Longitudinal studies are needed to identify algorithms best able to predict new-onset HTN risk over an extended period.

5.1.2. *Signal processing*

Within the category of signal processing approaches, PPG has been among the most frequently used modalities. PPG utilizes optical sensors to detect blood volume changes during the cardiac cycle and can be non-invasively measured from sites like the finger, earlobe, or wrist. From Table A2 it is observed that a multitude of methods were explored for medical data analysis, focusing primarily on predicting BP values. Among these, various ML techniques and CNN-LSTM displayed moderate accuracy at 67.8%, with a sensitivity of 68.4% and specificity of 66.6% [194]. Contrastingly, Filtering-CNN demonstrated improved performance, achieving an accuracy of 74.5%, indicating its potential for more precise BP estimations [99]. Holdout GoogLeNet emerged as a standout performer, showcasing impressive sensitivity (95.8%) and specificity (96.0%) for BP classification [84]. Similarly, EfficientNet, when combined with XG Boost for classification, exhibited an exceptional accuracy of 99.5% in 10 folds, signifying its robustness in handling BP-related data [195]. The utilization of diverse transforms such as synchro-squeezing, wavelet, and variational mode decomposition showcased competitive accuracies and lower errors in BP estimations. For instance, wavelet scattering transform combined with SVM resulted in an accuracy of 71.42% and an F1-score of 76%, highlighting its potential in BP prediction [90]. Ensemble methods like RF and AdaBoost illustrated strong performances in certain scenarios,

indicating their efficacy in handling complex physiological data. RF, for example, displayed an accuracy of 99.4% in Holdout, showcasing its potential for accurate BP prediction [100]. The models combining various methodologies or features exhibited promising outcomes. Fusion models integrating frequency spectrum features with CNN displayed lower errors in BP estimations. For instance, the fusion model showcased a Standard Deviation (SD) of 7.25 mmHg and Mean Absolute Error (MAE) of 5.59 mmHg for SBP, emphasizing the potential benefits of amalgamating different techniques for more accurate predictions [92]. Despite these advancements, some models demonstrated room for improvement. The Signal Morphology model, based on DTs, exhibited moderate accuracy at 69.9%, emphasizing the need for further refinement or additional features for better performance in BP prediction [95].

However, not all methodologies yielded equally promising outcomes. For instance, the CNN model in conjunction with Continuous Wavelet Transform (CWT) achieved a lower accuracy of 90% in Holdout CNN. This suggests the need for refinement in implementing this particular combination for BP estimation [196]. In conclusion, these diverse methodologies in medical data analysis underline the complexity of healthcare data and the critical role of ML in predicting physiological parameters, especially BP. Each approach showcased distinct strengths and weaknesses, calling for continuous research and potential integration of techniques to enhance prediction accuracy and reliability in medical diagnostics and monitoring.

ECG has also been widely applied to extract cardiac features informative for HTN. Various ML techniques were explored for medical data analysis, with diverse predictive performances noted, especially for cardiac and BP measurements. As shown in Table A3, the CART model exhibited an overall prediction success of 70.1% with a ROC area under the curve of 0.64, indicating moderate accuracy in classification tasks related to cardiovascular data [108]. Different transform methods such as Wavelets, Shearlets, and Contourlets were employed, displaying varying accuracies in their RF implementations. Contourlets outperformed the others with an accuracy of 91.32%, emphasizing its potential for more precise signal processing in cardiac data analysis [197]. An innovative approach utilized non-linear Empirical Mode Decomposition (EMD) combined with supervised KNN classification, achieving a high accuracy of 97.70% [104]. This method demonstrated robustness in signal decomposition and feature extraction, leading to the accurate classification of cardiac data. DL techniques, particularly two-stage DNN, showcased impressive accuracy metrics. The first stage achieved an average accuracy of 99.68% with high sensitivity and specificity, while the second stage maintained a respectable average accuracy of 90.98%, indicating a robust performance in cardiac data analysis, albeit with slightly lower sensitivity [111]. Individual CNN models demonstrated varying degrees of performance. Some achieved high AUC scores (0.96) with decent sensitivity and specificity, while others ranged between 68% and 90% accuracy, suggesting differences in architecture or training approaches [198].

Ensemble methods, such as utilizing optimal bi-orthogonal wavelet filter banks with bagged trees classifiers, showcased exceptional area under the curve of 1.00 and classification accuracy of 99.95%, highlighting the potency of ensemble learning for accurate predictions in cardiac data analysis [106]. Composite neural networks incorporating multiple architectures and graphics information demonstrated promising results with varying mean absolute errors for systolic and DBP. While these errors varied based on dataset size, the approach showed potential for accurate BP estimation. Additionally, feature selection methodologies like RA-ReliefF and MPGA-BPN models exhibited relatively low mean absolute errors for both systolic and DBP, indicating the effectiveness of feature selection in improving prediction accuracy [199]. However, some models demonstrated moderate performance, such as CNN with Residual Connections and CNN with LR, showing AUC scores of 0.845 and 0.92, respectively, suggesting room for improvement or optimization in these architectures for cardiac data analysis [114,115]. Overall, these diverse approaches highlight the evolving landscape of ML techniques in cardiac data analysis, underscoring the need for tailored methodologies to accurately predict and classify cardiovascular parameters. The variations in model performance indicate the necessity for continued research and refinement to achieve higher accuracy and reliability in diagnosing cardiac conditions and monitoring patient health.

Other common signals investigated include HRV derived from ECG or PPG recordings. This biosignal offers practical, inexpensive opportunities to passively monitor HTN indicators continuously over time through extracted pulse, heart rate, waveform morphology and variability-based features. The examination of HRV features, specifically through statistical analysis using SPSS, highlighted a reduction in HRV among subjects with HTN, suggesting potential implications for cardiovascular health. This observation was further supported by studies indicating reduced HRV in high-risk HTN subjects. Classification models trained on HRV features demonstrated varying degrees of accuracy. Some models achieved exceptional results, such as those attaining 100% accuracy, sensitivity, and specificity in classifying low and high-risk HT subjects (please refer to Table A4). Similarly, HRV time and frequency domain feature-based models showcased high accuracy, ranging from 96.7% to 97.08%, signifying the robustness of these features in classification tasks related to cardiovascular health [122]. However, not all classification models yielded equally high accuracies. For instance, a statistical analysis based on HRV parameters of 139 subjects achieved an accuracy of 85.7%, indicating relatively lower performance compared to other models [200]. This variation might stem from the complexity of HRV patterns among a larger and potentially more diverse subject group. Employing multidimensional HRV features alongside wavelet transform, ApEn, and SeEn revealed a promising classification accuracy of 93.3% [201]. This signifies the potential of combining various HRV features and signal processing techniques for accurate classification tasks associated with HRV data. Overall, the analysis of HRV features and their application in classification tasks showcased the potential of these metrics in discerning cardiovascular health conditions. While some models demonstrated outstanding accuracy, others showed slightly lower performance, highlighting the complexity of HRV data interpretation and the need for comprehensive feature selection and model optimization for precise classification and risk assessment in cardiovascular health studies.

Finally, BCG measures body movements caused by cardiac ejection of blood. BCG utilizes sensors to detect subtle displacements and vibrations transmitted through the body caused by the heart contracting and blood flow within the vasculature. Various ML techniques and signal processing methods were explored to predict BP values. The results showcased diverse performances across different models and approaches. The neural network model exhibited a moderate level of accuracy, with a MAE and standard deviation of 3.90 ± 4.79 mmHg for diastolic pressure and 4.62 ± 6.00 mmHg for systolic pressure, indicating some variability in accuracy and potential inconsistency in BP estimations using this architecture [202]. On the other hand, the TQWT coupled with a KNN classifier displayed robustness in classification tasks related to BP, achieving an accuracy of 92.21%, along with high sensitivity and specificity metrics, indicating its efficacy in accurately categorizing BP data [129]. Utilizing ensemble techniques with wavelet transform and extraction of non-linear features achieved an average classification accuracy of 89%, demonstrating promising performance in predicting BP values, though slightly lower compared to some other methods [130]. DL techniques, particularly deep CNN with Gabor transform and Continuous Wavelet Transform, demonstrated high classification accuracies ranging from 86.14% to 97.65% [131,132]. These approaches highlighted the potential of DL architectures in accurately estimating BP values from physiological data. The ConvMixer and Spectrogram techniques showed exceptional accuracies, ranging from 97.69% to 98.79% across different architectures (ResNet18, ResNet50, ConvMixer), underlining their effectiveness in BP estimation tasks [128] (please refer to Table A5).

While some methods demonstrated high accuracies and robustness in classification tasks, others showed moderately high errors or slightly lower accuracy rates. These findings highlight the computational approaches for this application area and suggest opportunities for additional research efforts. Fig. 10 shows the summary of results using various ML and DL approaches.

5.1.3. Fused data processing

The fusion of modalities for predicting physiological parameters, especially BP and cardiovascular health, showed varying performances. Combining ABP with PPG exhibited high sensitivity (93.1%) but lower specificity (76%) in a Holdout CNN model, indicating challenges in distinguishing patterns accurately [134]. PPG and HRV fusion achieved an F1-score of 83%, effectively categorizing HTN, and indicating promise in cardiovascular health assessment [203]. The fusion of PPG and ECG data revealed diverse accuracies, implying complexities in estimating BP with MAE and standard deviations. Different architectures combining ECG and PPG signals demonstrated varying accuracies and errors, highlighting the significant impact of fusion techniques and architectures on BP estimations. Fusion techniques using ECG and PPG, coupled with feature extraction and classification methods, displayed varied MAEs for BP measurements [119,120,135,136,204–206]. Integrating HRV features with ECG or BCG data showed accuracies ranging from 84.4% to 99.99% in cardiovascular health classifications, emphasizing the need for robust fusion techniques and models for accurate estimations [56,105].

Studies were also conducted by retrospectively collecting the data from Electronic Medical Records (EMRs) from a hospital [36,141]. The study utilized 79 different indicators such as 2 demographic, 4 comorbidity indicators, etc. The study used XGB to identify the etiologies in the patients with probable HTN. For the validation set the study attained AUC of 0.924. This study signifies the possibility of detecting the etiologies for secondary HTN with ML models using the EMRs which are normally available in hospitals. This might help the clinicians in early decision-making [36]. The studies are also conducted by collecting data from wearable smart devices making the data collection process future-ready [37]. In essence, fusion methods offer promise in understanding cardiovascular health parameters. These findings stress the importance of tailored fusion techniques and robust models for precise estimations and classifications in cardiovascular health assessment (please refer Table A6).

5.2. Assessment of secondary effects of HTN

The mechanism of HTN is complex and involves multifactorial effects. One impact involves changes in small arteries and arterioles, where structural alterations in blood vessels increase peripheral vascular resistance - a precursor to elevated BP [4]. Given its multifaceted pathophysiological mechanisms and asymptomatic nature in many cases, predicting and diagnosing HTN presents challenges for those most affected. In this context, medical imaging can help in visualizing the vascular changes in the brain and assessing structural changes in the heart, kidney, and eyes [50]. This requires revolutionary work on AI-based models in the prediction, diagnosis, and assessment of HTN patients using a multimodality approach.

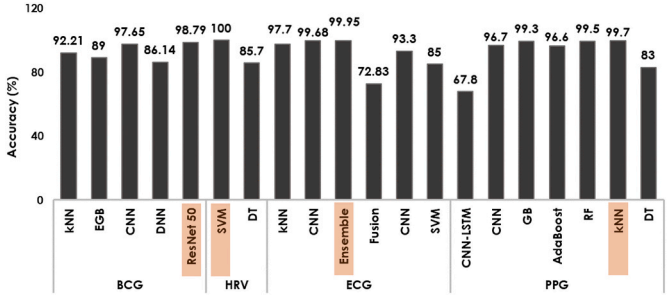

Fig. 10. Summary of accuracy (%) obtained using various ML and DL techniques with physiological signals for automated HTN detection.

5.2.1. Image processing

Within the category of image processing, several anatomical sites have been examined. Brain imaging modalities like MRI and CT have been used to identify subtle structural changes in the brain associated with HTN. Cardiac US provides insight into LVH and cardiac structure/function. Retinal fundus photography can detect microvascular changes in the retina linked to hypertensive retinal disease. These anatomical imaging approaches complement functional biosignals data by evaluating HTN-induced morphological impacts detectable through medical images.

From Table A7, it is noted that studies have proved that ML-based techniques are showing promising results in the prediction of HTN. A study by Ref. [158] has performed automated segmentation of vascular trees. They compared the classification results of six different classifiers and reported 100% accuracy for the ensemble (RUSBoosted) classifier for the whole brain region. The study also analyzed the prediction of HTN from the Anterior and posterior brain only and noticed that the vascular changes occurring on the anterior side are more helpful in the prediction of HTN than the ones on the posterior side. A study by Ref. [163] captured the MRA and BP measurements of 342 subjects. The cerebrovascular structures were segmented initially segmented using discrete Gaussians. Further, the missed small vessels were captured using 3D adaptive segmentation. Vasculature was obtained using a 3D region growing technique. This study attained a dice similarity coefficient of 92.23%, 94.82% sensitivity, and 99.0% specificity for segmentation. Further, the modifications in diameters of blood vessels and tortuosity were extracted and a feature vector was developed. This study generated synthetic data using the SMOTE. Finally, the features were fed to various classifiers, and using the AdaBoost ensemble the study achieved a maximum accuracy of 95.2% [163]. This also explored the significance of systole and diastole measurement individually in the diagnosis of HTN and observed that the measurement of Mean arterial pressure (MAP) was better from both these measurements. Studies have also used CNN for segmentation and SVM for classification and attained an accuracy of 90% [160].

It can be observed from Table A8 that ML techniques are performing well in the prediction of HTN from the US images of the heart. A study was performed by Ref. [39] on 61 patients with HTN and 51 normal patients. This study applied various feature transformation techniques to highlight meaningful details in the images. A large number of features were generated but processing all of them would be tedious. It employed LSDA for feature reduction. Various combinations of transforms and classifiers were tested, with the best results being 99.11% accuracy using shearlet and contourlet transforms with a DT classifier. Contourlet transforms achieved 100% specificity while shearlet transforms obtained 100% sensitivity. A major advantage is that only two features are needed for prediction, making the approach suitable for clinical applications using low-powered embedded systems. DL studies have also shown promise, with an ensemble of convolutional networks attaining 97.6% accuracy and 100% sensitivity for pulmonary arterial hypertension detection [167]. Echocardiogram is used in diagnosing cardiac hypertrophy from HTN and there exists a correlation of ATG9a with left ventricular posterior wall thickness [164]. PH can also be found in newborns and infants with several cardiac, and systemic diseases which may lead to morbidity and mortality. Being a non–invasive technique echocardiography is one of the recommended techniques by pediatricians for PH detection for these babies. A multi-view ECHO was collected by Ref. [168] study for the prediction of PH in newborns. The data was collected from 194 newborns. The study proposed spatiotemporal convolutional architectures and attained an F1-score of 0.84 & 0.92 for severity prediction & binary detection respectively.

The retinal vasculature could also be an indicator of the status of other vessels of the human body. Retinopathies accompanied by systemic illnesses like HTN and diabetes are common these days. A regular ophthalmological check-up could be the best approach to reduce the risk. Studies are conducted to classify HRT using retinal fundus images and attained the accuracy, sensitivity, and specificity of 99% each and AUC of 0.99 using TL-based mobile-net architecture [181]. One of the major stages in the prediction of HTN is segmentation. In a study by Ref. [173] retinal vessel calibers were extracted by using principal component analysis and mathematical morphological techniques. Further, these images were processed to identify the vascular tree. Then Bifurcation angle and the Vessel caliber were computed. The study attained an accuracy of 94.17% for segmentation on the DRIVE dataset. Also, it attained a classification rate of 61% for the prediction of HTN. The pre-processed images captured from the Chinese population dataset were given as input to the pre-trained Inception V3 model and the feature vector was developed. A classifier with fully connected and softmax layers was trained for classification. The study attained an accuracy of 68.8% and an AUC of 0.766 for HTN detection [172]. The drawback of this model is that it has a small dataset used for evaluation. Retinal analysis is dependent on the field of view of the camera used. With fundus camera with 45^0 can only cover a circular area up to 4 mm from the centre of the image. With the help of Ultra-widefield imaging with a scanning laser ophthalmoscope a wide area of retina can be covered. This helps to explore the vessel parameters in more regions than previously examined [174]. A study in Ref. [174], used these ultra-widefield images of the retina. They used Nasal–Annular Arteriole: Venule Ratio (NA-AVR) by considering the larger periphery of the retina. The outline of the location of the optic disk was manually annotated by an expert. Further with the help of scaled filters retinal vessels were segmented automatically. The average distance between parallel splines that were automatically fitted was used to determine the caliber (in microns) for each vessel segment in the measurement zone. It was observed that the NA-AVR ratio was higher in normotension in comparison with HTN. The limitation of this study is that it needs human intervention in the early stages thus leading to the possibility of bias. It can be observed that the applicability of ML models is not much explored in this field. Fig. 11 shows the highest performance of various techniques using imaging modalities.

Recently, it is observed that KNN has achieved promising results, when using US images [207]. As can be seen in Table A7 – A9, most studies were conducted on private datasets which were not very large. Hence, the generalization of these methods needs to be assessed on a larger dataset before clinical use. Longitudinal datasets featuring follow-up scans could provide more robust insights, clearly showing vessel changes over time. However, scans like MRA may be difficult to obtain repeatedly due to cost.

In the field of prediction using retinal fundus images applicability of ML models is not explored much. Pre-processing and segmentation are major parts of image-based analysis. Most of the studies have explored

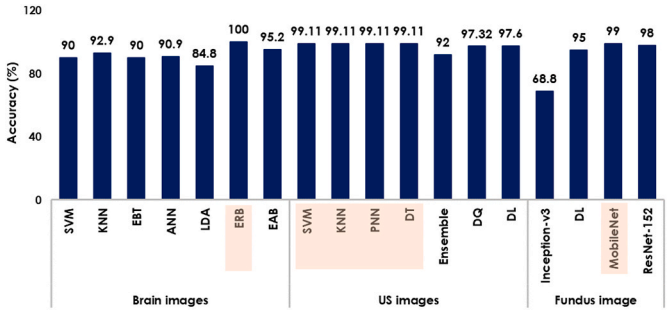

Fig. 11. Summary of accuracy (%) obtained using various ML and DL techniques with medical imaging modalities used to assess the secondary effects of HTN.

histogram and region-based techniques. However, Edge-based techniques might give good results in automatic segmentation.

Timely detection of secondary HTN causes through clinical assistance has significant value, as it may enable faster treatment and lowered BP outcomes. While numerous clinical studies investigate this important domain, applications of ML models require more exploration to aid practitioners' early detection capabilities. Larger, standardized datasets would advance such research and model validation efforts.

5.3. Challenges and future directions

While several studies have aimed to automatically detect HTN, there remains a lack of comprehensive work leveraging various data modalities for HTN assessment. Additionally, no studies have yet correlated risk factors with physiological signals and their effects on organs such as the brain, eyes and heart. Connecting these diverse types of clinical information poses significant challenges. Therefore, large-scale, multicenter socio-demographic studies are needed to capture HTN-related risk factors, biosignals and medical images. This would allow the development of robust prediction models for early detection and evaluation of the condition.

Some critical future directions are outlined below to help researchers to strengthen HTN identification in clinical decision-support tools. Comprehensively integrating relevant data domains through coordinated efforts could advance the state of the art. More holistic modeling approaches leveraging diverse, linked datasets offer promise for improved understanding and management of this major health concern.

Multimodality approach: In the realm of ML models, achieving robust detection, identification, and classification demands a comprehensive database comprising a diverse data modality. Integrating signals like PPG, ECG, BCG, and HRV, among others, lays the foundation for a multi-dimensional understanding of physiological responses [208]. These physiological signals, each offering unique insights into the body's functioning, form a critical component. Leveraging imaging data sourced from vision transformers, CNNs, and other techniques enriches the spectrum by unveiling hidden patterns within complex visual information. This fusion of signals and imaging data serves as a gateway to unravel intricate connections and correlations, reinforcing the depth and accuracy of the analysis. However, the holistic view remains incomplete without the incorporation of clinical information. Numerical data encompassing vital metrics like heart rate, SpO2, diastolic, and SBP are invaluable puzzle pieces that contribute significantly to the comprehensive understanding of health dynamics. The synergy between multimodal data sources strengthens ML models, enabling more robust interpretations and informed decisions. Integrating diverse data types represents progress in boosting predictive accuracy and resilience, with the potential to deliver more reliable, nuanced and comprehensive outcomes for medical diagnostics and other applications.

Use of novel image-based features: Advancements in image-based information extraction through cutting-edge models like Vision transformers [209] and CNNs, or even a blend of both, present an exciting frontier in predictive analytics. These learning architectures excel in extracting intricate patterns and relationships within imaging data, paving the way for remarkably accurate predictions. The utilization of such models not only enhances the extraction of critical features from images but also complements the insights derived from other modalities, enriching the predictive capabilities exponentially. Incorporating an image-based dataset fortified by these advanced learning models stands as a potent asset, offering a treasure trove of visual cues and hidden patterns that can significantly elevate the precision and depth of predictions across a spectrum of applications, especially in healthcare and diagnostic realms.

Uncertainty Quantization (UQ) and explainable AI (XAI): UQ and XAI stand as pivotal pillars in advancing the reliability and interpretability of AI systems. UQ involves the assessment and articulation of uncertainty levels within AI predictions like Bayesian techniques (e.g.

Markov chain Monte Carlo, Monte Carlo dropout), ensemble techniques (e.g. deep ensembles), and other techniques (e.g. variational inference, Laplace approximations), acknowledging the inherent uncertainty of real-world data [210,211]. Probabilistic techniques are used to quantify uncertainties in predictions, allowing AI systems to express confidence or ambiguity levels. Meanwhile, XAI aims to demystify complex models by elucidating the decision-making process. It seeks to promote transparency by providing understandable insights into how and why particular conclusions are reached. Explainable methods can help provide transparency around model interpretations and outcomes. The study [212] categorizes XAI methods into knowledge-driven and data-driven approaches and reviews concepts like the scope of explanations, principles of XAI, properties of good explanations, and key challenges. It outlines a taxonomy for XAI methods using four approaches: functioning-based, result-based, conceptual, and mixed. The study [213] investigates SHAP [214], GradCAM [215], Local Interpretable Model-agnostic Explanations (LIME) [216], Explainable Boosting Machine (EBM) [217], Case-Based Reasoning (CBR) [218], and Rule-Based Systems. In summary, by combining UQ with XAI methodologies, we not only enhance the reliability of AI predictions by acknowledging uncertainty but also empower users to comprehend and trust AI-driven decisions, fostering a symbiotic relationship between human understanding and machine intelligence.

Internet of Thongs (IoT): As a futuristic procedure for biomarker sensing and disease detection (as depicted in Fig. 12), we present a scenario through the integration of IoT-based sensors into everyday wearable devices which has revolutionized healthcare in unprecedented ways. Smartwatches, embedded with advanced biosensors, constantly monitor an individual's vital signs. As wearables collect this continuous stream of data, it is instantly transmitted to a secure and sophisticated cloud-based database. Here, powerful ML algorithms analyse this influx of information, utilizing predictive models to establish personalized baselines for everyone. These models continuously adapt and learn from the data, identifying patterns and deviations from normal parameters with remarkable accuracy. This comprehensive dataset, combined with AI-driven analytics, enables the early detection of potential health issues and allows for proactive interventions. This remote-based monitoring and health triage detection system has significantly reduced the burden on healthcare facilities and improved patient outcomes. Routine check-ups have become more efficient and personalized, as doctors can focus on high-priority cases while remotely guiding patients with minor issues. The future of healthcare revolves around this seamless integration of IoT-based sensors, cloud databases, machine learning, and remote connectivity [219]. We foresee that preventive healthcare will take centre stage, empowering individuals to take charge of their well-being while fostering a more collaborative and proactive approach to medicine.

6. Conclusion

In this systematic review, we analyzed 122 relevant articles from major academic databases. Our findings show that ML and DL techniques have been applied to detect HTN using clinical data, physiological signals, and fused clinical-signal approaches. Imaging modalities have also leveraged various ML and DL methods to assess the secondary effects of HTN. We have examined the datasets and techniques used in prior work. A summary of techniques used to develop HTN prediction models was also provided. ML approaches have been widely adopted across all domains. However, DL techniques are gaining popularity as they integrate feature extraction and classification in an end-to-end manner. The review also highlighted that the overall system performance could be improved through multimodal data and feature fusion. Finally, we discussed potential future research avenues aimed at strengthening AI model impact, reliability, and clinical relevance

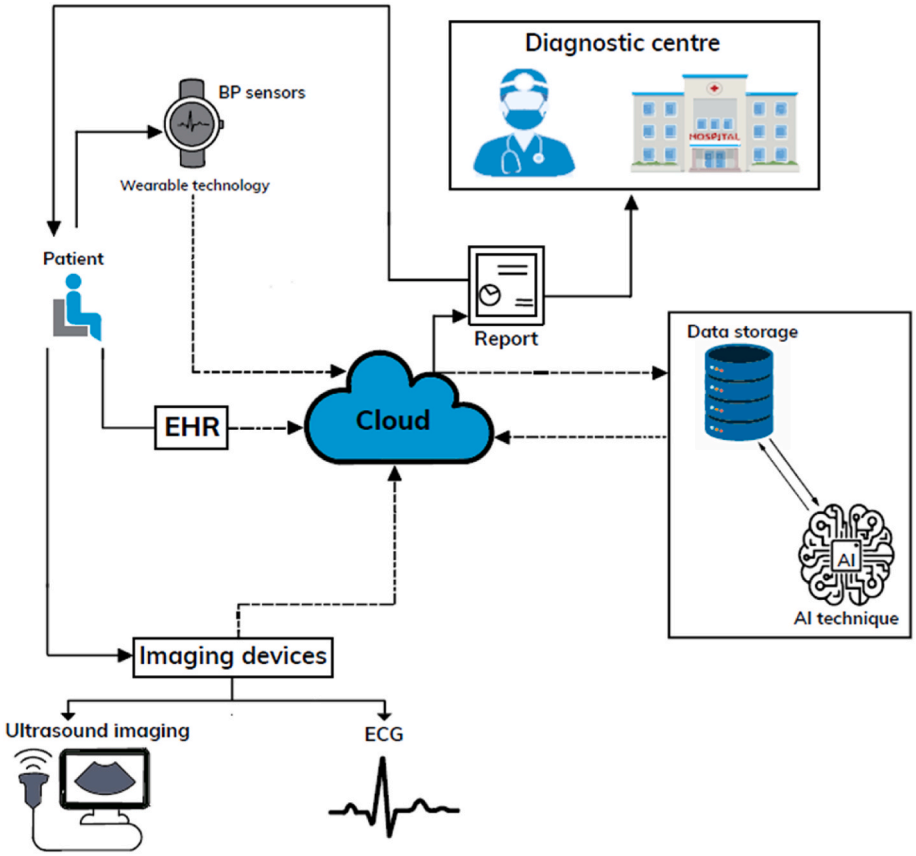

Fig. 12. Illustration of an IoT-based process for continuous remote monitoring and detection of HTN.

through more comprehensive modeling approaches.

CRediT authorship contribution statement

Anjan Gudigar: Writing – original draft, Writing – review & editing, Methodology, Investigation, Formal analysis, Data curation, Conceptualization, Visualization, Funding acquisition. **Nahrizul Adib Kadri:** Methodology, Data curation, Supervision. **U. Raghavendra:** Validation, Resources, Funding acquisition, Formal analysis, Data curation, Conceptualization. **Jyothi Samanth:** Writing – original draft, Resources, Formal analysis. **M. Maithri:** Writing – original draft, Resources, Formal analysis, Validation. **Mahesh Anil Inamdar:** Writing – original draft, Resources, Formal analysis, Validation. **Mukund A. Prabhu:** Validation. **Ajay Hegde:** Validation. **Massimo Salvi:** Writing – review & editing, Data curation, Conceptualization. **Chai Hong Yeong:** Writing – review & editing. **Prabal Datta Barua:** Writing – review & editing. **Filippo Molinari:** Writing – review & editing, Validation, Formal analysis. **U. Rajendra Acharya:** Writing – review & editing, Validation, Supervision, Data curation, Conceptualization.

Declaration of competing interest

The authors declare that they have no known competing financial interests or personal relationships that could have appeared to influence the work reported in this paper.

Acknowledgment

This research work is carried out under the SERB International Research Experience Fellowship for the year 2023–2024 supported by the Science and Engineering Research Board (SERB), a statutory body of the Department of Science and Technology, Government of India (FILE NO. SIR/2022/000809).

Appendix A. Summary of results

See Tables A1-A9.

Table A1
Summary of ML-based methods used to classify HTN using clinical data/ parameters.

Sl. No.	Paper	Dataset	Attributes	Method	Result
1.	[70]	Students:400	BMI, waist and hip circumference, and waist-hip ratio (WHR)	Classification tree	Misclassification error rate = 0.16
2.	[33]	Participants:1692		ANN	Acc.: 100%–23% (one missing value)
3.	[69]	MIMIC-II Records:446	HR, BP, and pulse volume	Fuzzy c-means clustering (FCM)	Acc.:92.51%, Sen.:94.53%
4.	[71]	CPCSSN Patients: 185,371 Controls:193,656	11	Neural network	Acc.:82%
5.	[34]	NHIC Patients:4707	BMI, DBP, total cholesterol and family history	Various ML methods are used	Acc.: 80.23%, F1-score: 0.8002 (for SVM)
6.	[66]	MIMIC II	8	CNN	Acc.: 89.95%
7.	[75]	HTN: 34,232 records	Textual + Numerical	BiLSTM +autoencoder	Acc.:89.7%
8.	[35]	PPG-BP (PPG not used)	Age, height, weight, systolic, BP, DBP, HR, Sex, and BMI (8 features)	Various ML methods are used	Acc.:99.5% (for C4.5 DT classifier & RF)
9.	[220]	NHANES Samples:24,434		Neural Network	Sen.:40%, Spec.: 87%, Prec.: 57.8%, AUC: 0.77
10.	[191]	Participants: 8,18,603, HTN: 82,748		Various ML methods are used	Acc.:90%, F1-score: 95%, Recall:100%
11.	[77]	Internal validation: 970 patients External Validation:464 patients		SHAP + RF	Acc.:81.9%, Sen.:61.9, Spec.:88.7, NPV:87.2%, AUROC = 0.884
12.	[193]	Records:303	Measurement type:4	Multilayer feed-forward neural network	Acc.:90%
13.	[67]	Individuals: 20206	Dummy variable:28, Continuous variable:2	Various ML methods are used	Sen.:81.8%, Spec.: 62.9% (for RF)
14.	[74]	Records: 33,289	23	Combining KNN and LightGBM	Acc.:86%, Recall:92%
15.	[192]	Individuals:30,320	13	Various ML methods are used	Acc.:82.9%, Recall:89.6%, Prec.87.8%, F1-score:87.7%, AUC:0.829 (for LR)
16.	[73]	HTN:12658, Non HTN: 18842	Age, gender, BP, blood glucose, urea, and creatinine	SMOTE + KNN	Acc.:83.9%, Sen.: 83.3%, Spec.:85.1%, AUC:0.896
17.	[68]	Respondents:612	27	Boruta-based feature selection + ADASYN + XGB (SHAP)	Acc.:88.81%, Prec.: 89.62%, Rec.: 97.04, F1-score: 93.18%, AUC:0.894 (For XGB)

*Acc.: Accuracy, Sen.: Sensitivity, Spe.: Specificity, AUC: Area under curve, Rec.: Recall, Prec.: Precision.

Table A2
Summary of ML-based methods used to classify HTN using PPG signals.

Sl. no	Reference	Dataset	Modality	Method	Results
1	[194]	PPG-BP, Subjects: 219, Records: 657	PPG	Filtering, CNN-LSTM	Acc.: 67.8%, Sen.: 68.4%, Spec.: 66.6%
2	[99]	PPG-BP 219 subjects; Records: 657	PPG	Filtering - CNN	Acc.: 74.5%, Sen.: 73.4%, Spec.: 75.7%
3	[84]	MIMIC-II Records: 150	PPG	Synchro-squeezing transform Holdout GoogLeNet	Sen.: 95.8%, Spec.: 95.96%

(*continued on next page*)

Table A2 (*continued*)

Sl. no	Reference	Dataset	Modality	Method	Results
4	[98]	MIMIC-I Subjects: 39, MIMIC-II Records: 12000, MIMIC-III Subjects: 510	PPG	TQWT and RF	MAE ± STD in SBP and DBP 0.74 ± 2.42 and 0.35 ± 1.06 respectively
5	[221]	WESAD Subjects: 17	PPG	Holdout CNN	Acc.: 96.7%
6	[100]	MIMIC-II Instances: 526906	PPG	RF	F1 Score: 99.4%
7	[195]	PPG-BP and MIMIC	PPG	Efficient-Net for feature Extraction and XG Boost	Acc.: 99.5%
8	[86]	MIMIC-II Subjects: 441, Records: 1323	PPG	Whole-based feature, SVM Classification	DBP:0.187, MAP:0.067, SBP:-0.050
9	[87]	PPG-BP Subjects: 219, Records: 657	PPG	Variational mode decomposition + GBC	Acc.: 99.3%, Sen.: 98.7%, Spec.: 100%
10	[88]	Private Subjects: 10	PPG	Statistical features + AdaBoost	Acc.:96.6%, Sen.: 94.9%, Spec.: 97.4%
11	[89]	MIMIC-II Subjects: 32536	PPG	Nonlinear features + SVM	Acc.: 70%, Sen.: 50%, Spec.: 75%
12	[222]	Vital DB Subjects: 3301	PPG	Physiological parameters Holdout CNN	Sen.: 80.7%, Spec.: 80.7%
13	[90]	NHANES	PPG	Wavelet scattering transform combined with SVM	Acc.:71.42% and F1-score: 76%
14	[91]	Private	PPG	Autocorrelation and FFT-based methods for estimating heart rate	
15	[110]	Private 200 subjects	PPG	CNN and LSTM	Estimated the mean and SD error for SBP: +1.91±5.55 mmHg and DBP: +0.67±2.84 mmHg
16	[92]	MIMIC II	PPG	Spectrum features and a specific fusion module with CNN	SD and MAE of the fusion model SBP:7.25 mmHg and 5.59 mmHg; DBP: 4.48 mmHg and 3.36 mmHg
17	[223]	Private Patients: 109	PPG	Cuffless and continuous BP 65 PPG features	MAE for SBP: 4.59 mmHg, DBP: 2.47 mmHg (multiple linear regression)
18	[224]	MIMIC II	PPG	Receptive Field Parallel, LSTM Attention Shrinkage Network (RFPASN)	MAE of 1.63/1.59 (DBP) and 2.26/2.15 (SBP) mmHg for BP
19	[225]	MIMIC	PPG	Multi-scale fusion and Multi-task learning ANN (MSF-MTLNet)	Mean and SD of estimation error for SBP: 0.97 ± 8.87 mmHg, DBP 0.55 ± 4.23 mmHg
20	[101]	MIMIC II	PPG	Hybrid LSTM-ANN model	MAE ± SD SBP 3.39 ± 5.47 mmHg, DBP 1.79 ± 3.72 mmHg
21	[93]	Private Records:657,Patients: 219, Normal: 237, Pre-HTN 258, HTN Type-I 102, HTN Type-II 60	PPG	Discrete wavelet decomposition	Classification NT vs. diabetic patients Acc: 99.1% NT vs PHT F1 score:92%, 83.1% NT vs.HT-I F1 score: 98.5%, 95.6% NT vs HT-II F1 score: 98.3%, 86.8% SBP and DBP respectively
22	[226]	MIMIC III	PPG	RF + GWO-GBRT	MAE and SD: SBP 2.91 mmHg and 3.97 mmHg, DBP 1.71 mmHg and 2.35 mmHg.
23	[227]	MIMIC II	PPG	Poincar'e-based feature extraction	SBP and DBP: 0.79 ± 3.08 and 1.38 ± 4.53 mmHg, respectively (for GPR)
24	[228]	PPG-BP Subjects: 219;	PPG	k-fold CV DT, Holdout CNN-LSTM	Acc.: 99.5 %(Best)
25	[196]	MIMIC-III Subjects: 30000 Records: 67830	PPG	CWT Holdout CNN	Acc.: 90%
26	[94]	Private Subjects: 121; Records: 700 HTN and 709 Normal	PPG	EMD + KNN	Acc.: 99.4%, Sen.: 99.6%, Spec.: 99.2%
27	[95]	PPG-BP and MIMIC - III Subjects: 219 and 140 resp	PPG	Signal morphology, DT	Acc.: 69.9%, Sen.: 66.7%, Spec.: 71.1%
28	[96]	Subjects:121 subjects from the PPG–BP fig share database	PPG	BP feature with KNN	F1-score:100%
29	[137]	MIMIC, Subject: 121	PPG	CWT Classification using Pre-trained CNN	F1-score:92.55%
30	[50]	Private, Subject:124	PPG	Waveform features	Sen.:85.71%, F1-score:92.31%
31	[97]	Public Dataset Subjects, Normal: 45, PHT: 58, HTN: 45	PPG	Ensemble EMD with SVM	Acc.: 89%, Sen.: 81%, Spec.: 85%

*DBP: Diastolic Blood Pressure, SBP: Systolic Blood Pressure, MAP: Mean Arterial Pressure, FFT: Fast Fourier Transform, PHT: Pre-hypertension, ANFIS: Adaptive network-based fuzzy inference system, HT-I: Hypertension type 1, HT-II: Hypertension type 2, GPR: Gaussian process regression, MAE: Mean absolute error, GBC: Gradient boosting classifier.

Table A3
Summary of ML-based methods used to classify HTN using ECG signals.

Sl. no	Reference	Dataset	Modality	Method	Results
1	[108]	Private Subjects:235 IPF	ECG	CART	Acc.: 70.1%, AUC: 0.64
2	[197]	MIT-BIH data set	ECG	Transform Wavelets, Shearlets and Contourlets with RF	Acc.: 81.84% (Wavelets) Acc.: 82.97% (Shearlets), Acc.: 91.32% (Contourlet)
3	[104]	SHAREE Subjects: 139, MIT-BIH	ECG	18 non-linear supervised KNN	Acc.: 97.70%,Sen.: 98.90%,Spec.:=89.10%

(*continued on next page*)

Table A3 (*continued*)

Sl. no	Reference	Dataset	Modality	Method	Results
4	[111]	Physikalisch-Technische Bundesanstalt (PTB) diagnostic database	ECG	CNN	First stage Acc.: 99.68%, Sen.: 99.51%, Spec.: 100.00%, F1-score: 0.997, Kappa: 0.993. Second stage deep Acc: 90.98%, Sen: 85.92%, Spec: 96.00%, F1-score: 0.905, Kappa: 0.819.
5	[198]	Patients: 2448 HCM 51,153 non-HCM	ECG	CNN	AUC: 0.96 Sen.: 87%, Spec.: 90%
6	[106]	SHAREE database Patients: 139 HPT, PTB database Patients: 52 healthy	ECG	optimal bi-orthogonal wavelet filter bank with EBT	Acc.: 99.95%, AUC: 1.00
7	[229]	Cooking hacks 180° eMotion FAROS Zephyr Bioharness module Savvy sensor platform Charis Physionet database	ECG	Information Fusion	Acc.: 72.83%
8	[112]	Private	ECG	CNN	Acc.: 68–70%
9	[105]	MIT-BIH	ECG	FDM+KNN	Acc.: 99.91%
10	[113]	SHAREE	ECG	CNN and SVM classifier	Acc.: 93.33%
11	[114]	CODE Dataset	ECG	CNN with Residual Connections	AUC: 0.845
12	[115]	Private Patients: 99,252	ECG	CNN with LR	AUC: 0.92
13	[109]	Private	ECG	SVM	Acc.: 85%
14	[116]	Shinken Database	ECG	CNN	AUC: 0.92
15	[117]	Physiobank Long-Term AF Database	ECG	CNN and Transformer	AUC: 0.71 ± 0.02
16	[199]	UCI_BP dataset, Subjects: 522 and 23,608 sets of data	ECG	RA-ReliefF feature selection and MPGA-BPN models	The MAE ± SD of SBP: 2.59 ± 3.41 mmHg DBP: 2.69 ± 3.31 mmHg, respectively
17	[107]	SHAREE: Patients: 139	ECG	Signal fractal dimension and Log energy, Wavelet	Acc.: 100 % discrimination of LRHT, HRHT
18	[118]	Private	ECG	CNN	AUC: 0.89

*CART: Classification and Regression Trees, EBT: Ensemble bagged trees classifier.

Table A4
Summary of ML-based methods used to classify HTN using HRV signals.

SL.No.	Reference	Dataset	Modality	Method	Results
1	[121]	Private, Subjects: 60	HRV	HRV features Statistical analysis using SPSS	HRV reduce in HT subjects
2	230	SHAREE, Subjects 139	HRV	HRV features +RUSBoost	Acc.: 97.08%
3	[122]	Private, Patients :113	HRV	Nonlinear parameters + SVM	Acc.: 100%, Sen.: 100%, Spec.: 100%
4	[123]	Private, Patients: 185	HRV	Features (time & frequency) + SVM	Acc.: 96.7%
5	[124]	Private, Patients: 56	HRV	Features (time & frequency)	HRV decreased in HT group
6	[200]	SHAREE	HRV	Nonlinear features+RF	Acc.: 85.7%, Sen.: 71.4%, Spec.: 87.8%
7	[126]	SHAREE, Subjects:139	HRV	Wavelet transform + RF	AUC: 0.95
8	[201]	Private, Subjects: 24	HRV	Features (time & frequency) + SVM	Acc.: 93.3%

Table A5
Summary of ML-based methods used to classify HTN using BCG signals.

SL. No	Reference	Dataset	Modality	Method	Results
1	[202]	Private	BCG	Neural network	MAE and SD DBP: 3.90 ± 4.79 mmHg, SBP: 4.62 ± 6.00 mmHg
2	[129]	figshare link: https://doi.org/10.6084/m9.figshare.7594433	BCG	TQWT + KNN	Acc.: 92.21%, Sen.: 92.96%, and Spec.: 91.60%
3	[130]	Private	BCG	wavelet transform, non-linear features are extracted from the SBs of WT and IMFs of EMD and ensemble gentleboost (EGB)	Acc.: 89%
4	[132]	Private, Records (35 males and 32 females): 67	BCG	CNN and Gabor transform techniques	Acc.: 97.65%

(*continued on next page*)

Table A5 (*continued*)

SL. No	Reference	Dataset	Modality	Method	Results
5	[131]	Private Patients: 67 HC and 61 HPT	BCG	Continuous Wavelet Transform and ANN	Acc.: 86.14%
6	[128]	RS-611 link: https://doi.org/10.6084/m9.figshare.7594433	BCG	ConvMixer and Spectrogram Techniques	ResNet 50 Acc.: 98.79%, (Best)

Table A6
Summary of the studies performed using data fusion for the detection of HTN.

SL. No	Author and Year	Dataset	Modality	Method	Results
1	[134]	MIMIC III, Subjects: 50, Records: 635	ABP and PPG	CWT Holdout CNN	Sen.: 93.1%, Spec.: 76%
2	[203]	Private, Subjects: 20	PPG and HRV	Mean, STD, min and max, Features (time & frequency)	F1-score:83%
3	[204]	MIMIC II	PPG and ECG	Multi-filter to multi-channel	MAE and SD for DBP: 2.13 (2.47) and 3.07 (3.52) mmHg; SBP: 3.52 (4.18) and 5.10 (5.87) mmHg
4	[102]	Private	PPG and ABP	Shallow Neural Network	Sen.: 93%, Spec.: 88%, Acc.: 90%
5	[136]	MIMIC II	PPG and ECG	CNN LSTM	SBP and DBP is -0.17 ± 4.62 mmHg and -0.24 ± 2.95 mmHg
6	[135]	MIMIC III	PPG and ECG	Nested Attention-guided BiConvLSTM network	MAE for SBP: 2.63 mmHg, DBP:1.09 mmHg, MAP:2.37 mmHg
7	[231]	PPG-BP Subjects: 219, Records: 657	PPG and ECG	Holdout ResNet CNN	
8	[140]	Private, Subjects: 43	PPG and HRV	HRV time and frequency domain features	Acc.: 85.47%, Spec.: 83.33%, Prec.: 92.11%
9	[205]	UCI Machine Learning Repository MIMIC III Records: 12,000	ECG and PPG	PTT and PIR measurements	DBP : −0.09, MBP: −0.16, SBP: −0.29
10	[119]	MIMIC III waveform database	ECG and PPG	LSTM	MAE-0.22 ± 5.82 mmHg, -0.57 ± 4.39 mmHg, and -0.75 ± 5.62 mmHg for SBP, MAP, and DBP measurements
11	[206]	MIMIC II	ECG and PPG	Womersley number (feature extraction), BP, GA with the RF	MAE for SBP:13.53 mmHg, DBP:9.51 mmHg, MBP:6.70 mmHg
12	[120]	MIMIC III	ECG and PPG	CNN-LSTM network	MAE SBP:4.41 mmHg, DBP: 2.91 mmHg, MAP: 2.77 mmHg
13	[139]	MIMIC II	ECG and PPG	Hybrid neural network	MAE for SBP: 3.7 mmHg, DBP: 2.81 mmHg
14	[125]	Private, Subjects: 71	HRV and ECG	CWT, HRV feature	F1-score = 91.33%
15	[56]	128 Open source	HRV and BCG	Features (time & frequency)	Acc.: 84.4%, Prec.: 82.5%,
16	[127]	Private 18 subjects	BCG and HRV	Features (time & frequency) and DFA	Acc.: 92.3%
17	[133]	30 subjects	Echocardiography and ECG	strain & temporal features + SVM	Prec.:97.62%, Sen.:93.33%, F1-score:95.43%
18	[232]	Healthy:357 patients PH:405 patients	echocardiographic measures + Chest X-rays	Used various deep learning approaches such as Xception, Inception V3, and Resnet50,	AUC:0.97
19	[171]	142 patients	echocardiographic measures + Chest X-rays	DL approach	AUC: from 0.65 to 0.74 (for PH)
20	[37]	Hypertensive: 402, healthy: 128	ECG + location + weather condition + cardiovascular features	MLP, RF	Acc: 87.8%, Sensitivity: 88.1%, Specificity: 87.1% (for RF)
21	[36]	7532 patients	79 clinical indicators + CT reports	XGB	AUC: 0.924
22	[141]	200 patients	MRI of heart, kidneys, renal arteries, adrenals and aorta.	clinical + Kruskal-Wallis	

*GA: Genetic algorithm.

Table A7
Summary of the studies performed using MRA images for the detection of HTN.

Sl. No.	Paper	Dataset	Image Modality	Methods	Results
1	[162]	15 patients	MRA	3-D Local adaptive segmentation + Median vascular radius and Tortuosity + Correlation	Sen.:94.82%, Spec.:99%, DSC:92.23%,AVVD:10.03%
2	[160]	60 Subjects	MRA	3D - CNN + vessel diameters and tortuosity + SVM	Acc.:90%
3	[38]	Normotensive: 33 subjects Hypertensive:33 subjects	MRA	3D - CNN + diameters and tortuosity + ANN	Acc.:90.9%
4	[161]	190	MRA	Linear Combination of Discrete Gaussians (LCDG) + 3D connectivity	DSC: 89.06 ± 6.39
5	[158]	72 subjects	MRA	Linear Combination of Discrete Gaussians (LCDG)	Acc.:100% (for HTN)
6	[163]	342 subjects	MRA	3D adaptive region growing + diameters and tortuosity + Ensemble classifier	Acc.:95.2%

*MRA :Magnetic Resonance Angiography, DSC :Dice Similarity Coefficient, AVVD: Absolute Vessel Volume Difference.

Table A8
Summary of the studies performed using US images for the detection of HTN.

Sl. No	Paper	Dataset	Image Modality	Methods	Results
1	[165]	Normal:49 PH:49	Echocardiographic images	GWLBP + fuzzy entropy + SVM	Acc.:91.77%, Sen.:96%, Spec.:87.33%
2	[166]	90 patients	echocardiographic measures	RF of regression trees	AUC:0.87
3	[39]	Healthy:54 patients HTN:54 patients	Echocardiographic images	Shearlet and contourlet transform + LSDA + DT classifier	Acc.:99.11%
4	[167]	Normal:67 patients PAH:450 patients RV dilatation:308 patients	Echocardiographic images	Ensemble of deep convolutional networks	Acc.: 97.6 %, Sen:100% (for PH)
5	[168]	194 newborns	echocardiography videos/ echocardiograms	Spatio-temporal convolutional architectures	F1-score:0.84 & 0.92 (severity prediction & binary detection)
6	[169]	Normal:112 HTCM:185	Echocardiographic images	3-D ConvNet + weakly supervised feature ensemble module	Acc.:92%, Sen.:97%, Spec.:84%, AUC:0.90
7	[170]	PH: 346 patients	Echocardiographic images	Local features + ML model	AUC = 0.950
8	[164]	168 patients	ATG9a and US cardiogram	Showed a correlation of ATG9a with left ventricular posterior wall thickness	

Table A9
Summary of the studies performed using retinal fundus images for the detection of HTN.

Sl. No	Paper	Dataset	Used imaging	Methods	Results
1	[173]	DRIVE, Private: Normal:38 subjects, diseased:29	Retinal fundus images	Measurement of vessel calibers and bifurcation angles	Acc.:94.17%
2	[172]	625 participants	Retinal fundus images	InceptionV3	Acc.:68.8%, AUC:0.766
3	[174]	440 participants	Ultra-widefield imaging of retina	Scaled filters + supervised ML classifier	AUC: left eye: 0.73, right eye: 0.64
4	[179]	HRT:1600 Non-HRT:2670	Retinal fundus images	DenseHyper system + deep residual learning network	Acc. = 95%
5	[181]	HRT: 3410 Non- HRT:5760	Retinal fundus images	TL-based MobileNet architecture	Acc.:99%
6	[180]	HRT-NR:200, HRT-MD:200, HRT-MO:200, HRT-MG:200, HRT-SR:200	Retinal fundus images	Enhanced fuzzy C-means clustering + Improved loss function in ResNet152	Acc.:98%

Appendix B. Abbreviations

See Table B1.

Table B1
Abbreviations of Major terms

Abbreviations	Definitions	Abbreviations	Definitions
ABP	Arterial Blood Pressure	LightGBM	Light Gradient Boosting Machine
ADASYN	Adaptive Synthetic	LR	Logistic Regression
AE	Autoencoder	LSDA	Locality-Sensitive Discriminant Analysis
AI	Artificial Intelligence	LVH	Left Ventricular Hypertrophy
ANN	Artificial Neural Network	MAE	Mean Absolute Error
BCG	Ballistocardiogram	MIMIC-II	Multiparameter Intelligent Monitoring In Intensive Care II
BiLSTM	Bidirectional Long Short-Term Memory	ML	Machine Learning
BMI	Body Mass Index	MLP	Multi-Layer Perceptron
BP	Blood Pressure	MRA	Magnetic Resonance Angiography
CAD	Computer-Aided Diagnostic	MRI	Magnetic Resonance Imaging
CKD	Chronic Kidney Disease	NB	Naive Bayes
CNN	Convolutional Neural Network	NHANES	National Health And Nutrition Examination Survey
CPCSSN	Canadian Primary Care Sentinel Surveillance Network	NHIC	National Health Insurance Corporation
CT	Computed Tomography	NICOLA	Northern Ireland Cohort For The Longitudinal Study Of Ageing
CVD	Cardiovascular Disease	PAP	Pulmonary Arterial Pressure
CWT	Continuous Wavelet Transform	PH	Pulmonary Hypertension
DBP	Diastolic Blood Pressure	PPG	Photoplethysmography
DL	Deep Learning	PRISMA	Preferred Reporting Items For Systematic Reviews And Meta-analyses
DNN	Deep Neural Network	RF	Random Forest
DT	Decision Tree	SBP	Systolic Blood Pressure
ECG	Electrocardiography	SHAP	Shapley Additive Explanations
EHRs	Electronic Health Records	SHAREE	Smart Health For Assessing The Risk Of Events Via ECG
EMD	Empirical Mode Decomposition	SMOTE	Synthetic Minority Over-Sampling Technique
GBM	Gradient Boosting Machine	SD	Standard Deviation
GGMRF	Gauss-Markov Random Field	SVM	Support Vector Machine

(continued on next page)

Table B1 (*continued*)

Abbreviations	Definitions	Abbreviations	Definitions
GWLBP	Global Weighted Local Binary Pattern	TL	Transfer Learning
HCM	Hypertrophic Cardiomyopathy	TQWT	Tunable Q-Factor Wavelet Transform
HMOD	Hypertensive Mediated Organ Damage	UQ	Uncertainty Quantization
HRT	Hypertensive Retinopathy	US	Ultrasound
HRV	Heart Rate Variability	WoS	Web of Science
HTN	Hypertension	XAI	Explainable AI
KNN	K-Nearest Neighbour	XGB	Extreme Gradient Boosting
LDA	Linear Discriminant Analysis		

References

[1] Worldwide trends in hypertension prevalence and progress in treatment and control from 1990 to 2019: a pooled analysis of 1201 population-representative studies with 104 million participants, Lancet 398 (2021) 957–980.

[2] 2003 European Society of Hypertension-European Society of Cardiology guidelines for the management of arterial hypertension, J. Hypertens. 21 (2003) 1011–1053.

[3] W.H. Organization, et al., A global brief on hypertension: Silent killer, global public health crisis: world health day 2013, in: Tech. Rep., World Health Organization, 2013.

[4] S. Oparil, M. Acelajado, G. Bakris, D. Berlowitz, R. Cifkova, A. Dominiczak, Hypertension, Nat. Rev. Dis. Prim. 4 (2018) 18014.

[5] R. Kreutz, E. Abd el-Hady Algharably, Blood pressure control, in: S. Offermanns, W. Rosenthal (Eds.), Encyclopedia of Molecular Pharmacology, Springer International Publishing, Cham, 2021, pp. 317–322.

[6] G. Mancia, G. Grassi, The autonomic nervous system and hypertension, Circ. Res. 114 (2014) 1804–1814.

[7] G. Mancia, R. Kreutz, M. Brunström, M. Burnier, G. Grassi, A. Januszewicz, M. L. Muiesan, K. Tsioufis, E. Agabiti-Rosei, E.A.E. Algharably, M. Azizi, A. Benetos, C. Borghi, J.B. Hitij, R. Cifkova, A. Coca, V. Cornelissen, J.K. Cruickshank, P. G. Cunha, A.H.J. Danser, R.M. Pinho, C. Delles, A.F. Dominiczak, M. Dorobantu, M. Doumas, M.S. Fernández-Alfonso, J.M. Halimi, Z. Járai, B. Jelaković, J. Jordan, T. Kuznetsova, S. Laurent, D. Lovic, E. Lurbe, F. Mahfoud, A. Manolis, M. Miglinas, K. Narkiewicz, T. Niiranen, P. Palatini, G. Parati, A. Pathak, A. Persu, J. Polonia, J. Redon, P. Sarafidis, R. Schmieder, B. Spronck, S. Stabouli, G. Stergiou, S. Taddei, C. Thomopoulos, M. Tomaszewski, P. Van de Borne, C. Wanner, T. Weber, B. Williams, Z.Y. Zhang, S.E. Kjeldsen, 2023 ESH guidelines for the management of arterial hypertension the task force for the management of arterial hypertension of the European society of hypertension: endorsed by the international society of hypertension (ISH) and the European renal association (ERA), J. Hypertens. 41 (12) (2023) 1874–2071, https://doi.org/10.1097/HJH.0000000000003480. Epub 2023 Sep. 26.

[8] R. Rapport, Hypertension. Silent killer, N. J. Med. 96 (3) (1999) 41.

[9] C. Ye, T. Fu, S. Hao, Y. Zhang, O. Wang, B. Jin, M. Xia, M. Liu, X. Zhou, Q. Wu, et al., Prediction of incident hypertension within the next year: prospective study using statewide electronic health records and machine learning, J. Med. Internet Res. 20 (1) (2018) e22.

[10] C.M. McEniery, J.R. Cockcroft, M.J. Roman, S.S. Franklin, I.B. Wilkinson, Central blood pressure: current evidence and clinical importance, Eur. Heart J. 35 (2014) 1719–1725.

[11] P. Boutouyrie, A. Achouba, P. Trunet, S. Laurent, Amlodipine-valsartan combination decreases central systolic blood pressure more effectively than the amlodipine-atenolol combination: the EXPLOR study, Hypertension 55 (2010) 1314–1322 (Dallas, Tex: 1979).

[12] J.W.M. Lenders, M.N. Kerstens, L. Amar, A. Prejbisz, M. Robledo, D. Taieb, et al., Genetics, diagnosis, management and future directions of research of phaeochromocytoma and paraganglioma: a position statement and consensus of the Working Group on Endocrine Hypertension of the European Society of Hypertension, J. Hypertens. 38 (2020) 1443–1456.

[13] P. Mulatero, S. Monticone, J. Deinum, L. Amar, A. Prejbisz, M.C. Zennaro, et al., Genetics, prevalence, screening and confirmation of primary aldosteronism: a position statement and consensus of the Working Group on Endocrine Hypertension of the European Society of Hypertension, J. Hypertens. 38 (2020) 1919–1928.

[14] F. Fallo, G. Di Dalmazi, F. Beuschlein, N.R. Biermasz, F. Castinetti, A. Elenkova, et al., Diagnosis and management of hypertension in patients with Cushing's syndrome: a position statement and consensus of the Working Group on Endocrine Hypertension of the European Society of Hypertension, J. Hypertens. 40 (2022) 2085–2101.

[15] M.Z.I. Chowdhury, I. Naeem, H. Quan, A.A. Leung, K.C. Sikdar, et al., Prediction of hypertension using traditional regression and machine learning models: a systematic review and meta-analysis, PLoS One 17 (4) (2022) e0266334, https://doi.org/10.1371/journal.pone.0266334.

[16] G.F.S. Silva, T.P. Fagundes, B.C. Teixeira, et al., Machine learning for hypertension prediction: a systematic review, Curr. Hypertens. Rep. 24 (2022) 523–533, https://doi.org/10.1007/s11906-022-01212-6.

[17] M. Sharma, J.S. Rajput, R.S. Tan, U.R. Acharya, Automated detection of hypertension using physiological signals: a review, Int. J. Environ. Res. Publ. Health 18 (11) (2021) 5838, https://doi.org/10.3390/ijerph18115838.

[18] Erick Martinez-Ríos, Luis Montesinos, Alfaro Ponce, Mariel, Pecchia, Leandro, A review of machine learning in hypertension detection and blood pressure estimation based on clinical and physiological data, Biomed. Signal Process Control 68 (2021) 102813, https://doi.org/10.1016/j.bspc.2021.102813.

[19] C. du Toit, T.Q.B. Tran, N. Deo, S. Aryal, S. Lip, R. Sykes, I. Manandhar, A. Sionakidis, L. Stevenson, H. Pattnaik, S. Alsanosi, M. Kassi, N. Le, M. Rostron, S. Nichol, A. Aman, F. Nawaz, D. Mehta, R. Tummala, L. McCallum, S. Reddy, S. Visweswaran, R. Kashyap, B. Joe, S. Padmanabhan, Survey and evaluation of hypertension machine learning research, J. Am. Heart Assoc. 12 (9) (2023) e027896, https://doi.org/10.1161/JAHA.122.027896. Epub 2023 Apr 29. PMID: 37119074; PMCID: PMC10227215.

[20] A.V. Chobanian, G.L. Bakris, H.R. Black, et al., The seventh report of the joint national committee on prevention, detection, evaluation, and treatment of high blood pressure: the JNC 7 report, JAMA 289 (19) (2003) 2560–2571, https://doi.org/10.1001/jama.289.19.2560.

[21] R. Katakam, K. Brukamp, R.R. Townsend, What is the proper workup of a patient with hypertension? Cleve. Clin. J. Med. 75 (9) (2008) 663–672, https://doi.org/10.3949/ccjm.75.9.663. PMID: 18788227.

[22] Institute for Clinical Systems Improvement (ICSI), Hypertension Diagnosis and Treatment, Institute for Clinical Systems Improvement (ICSI), Bloomington, Minn, 2010.

[23] Stiles S. Framingham Criteria Predict New Hypertension Better Than Prehypertension in Young Adults. Medscape Medical News. Available at: http://www.medscape.com/viewarticle/811416. Accessed: September 30, 2013.

[24] A.P. Carson, C.E. Lewis, D.R. Jacobs Jr., C.A. Peralta, L.M. Steffen, J.K. Bower, et al., Evaluating the Framingham Hypertension Risk Prediction Model in Young Adults: the Coronary Artery Risk Development in Young Adults (CARDIA) Study. Hypertension, 2013 Sep 16.

[25] T. Koivistoinen, L.P. Lyytikainen, H. Aatola, et al., Pulse wave velocity predicts the progression of blood pressure and development of hypertension in young adults, Hypertension 71 (3) (2018) 451–456.

[26] B. Williams, G. Mancia, W. Spiering, E. Agabiti Rosei, M. Azizi, M. Burnier, et al., 2018 ESC/ESH guidelines for the management of arterial hypertension: the task force for the management of arterial hypertension of the European society of cardiology and the European society of hypertension: the task force for the management of arterial hypertension of the European society of cardiology and the European society of hypertension, J. Hypertens. 36 (2018) 1953–2041.

[27] S.V. Greve, M.K. Blicher, T. Sehestedt, E.M. Gram-Kampmann, S. Rasmussen, J. K. Vishram, et al., Effective risk stratification in patients with moderate cardiovascular risk using albuminuria and atherosclerotic plaques in the carotid arteries, J. Hypertens. 33 (2015) 1563–1570.

[28] M. Bombelli, R. Facchetti, S. Carugo, F. Madotto, F. Arenare, F. Quarti-Trevano, et al., Mean Absolute Error increases cardiovascular risk independently of in-office and out-of-office blood pressure values, J. Hypertens. 27 (2009) 2458–2464.

[29] D. Levy, R.J. Garrison, D.D. Savage, W.B. Kannel, W.P. Castelli, Prognostic implications of echocardiographically determined left ventricular mass in the Framingham Heart Study, N. Engl. J. Med. 322 (1990) 1561–1566.

[30] M.J. Koren, R.B. Devereux, P.N. Casale, D.D. Savage, J.H. Laragh, Relation of left ventricular mass and geometry to morbidity and mortality in uncomplicated essential hypertension, Ann. Intern. Med. 114 (1991) 345–352.

[31] A. Caroli, A. Remuzzi, L.O. Lerman, Basic principles and new advances in kidney imaging, Kidney Int. 100 (2021) 1001–1011.

[32] B.K. Park, Gray-scale, color Doppler, spectral Doppler, and contrast-enhanced renal artery ultrasound: imaging techniques and features, J. Clin. Med. (2022) 11.

[33] W. Seffens, C. Evans, Taylor Minority Health-Grid Network And Herman, Machine learning data imputation and classification in a multicohort hypertension clinical study, Bioinf. Biol. Insights 9 (2015) BBI–S29473.

[34] R. Patnaik, M. Chandran, S.-C. Lee, A. Gupta, C. Kim, C. Kim, Predicting the occurrence of essential hypertension using annual health records, in: 2018 Second International Conference on Advances in Electronics, Computers and Communications, ICAECC), Bangalore, India, 2018, pp. 1–5, https://doi.org/10.1109/ICAECC.2018.8479458.

[35] M. Nour, K. Polat, Automatic classification of hypertension types based on personal features by machine learning algorithms, Math. Probl Eng. 2020 (2020) 1–13.

[36] X. Diao, Y. Huo, Z. Yan, H. Wang, J. Yuan, Y. Wang, J. Cai, W. Zhao, An application of machine learning to etiological diagnosis of secondary hypertension: retrospective study using electronic medical records, JMIR Med Inform 9 (1) (2021) e19739, https://doi.org/10.2196/19739.

[37] Sladjana Jovanovic, Milan Jovanović, Ćeranić Škorić, Tamara, Stevan Jokic, Branislav Milovanovic, Konstantinos Katzis, Dragana Bajic, A mobile crowd sensing application for hypertensive patients, Sensors 19 (2019) 400–416, https://doi.org/10.3390/s19020400.

[38] H. Kandil, A. Soliman, F. Taher, M. Ghazal, A. Khalil, G. Giridharan, A. El-Baz, A novel computer-aided diagnosis system for the early detection of hypertension based on cerebrovascular alterations, Neuroimage: Clinical 25 (2020) 102107.

[39] U. Raghavendra, J.K. En Wei, A. Gudigar, A. Shetty, J. Samanth, G. Paramasivam, A.A. Ardakani, Automated Diagnosis and Assessment of Cardiac Structural Alteration in Hypertension Ultrasound Images, Contrast Media & Molecular Imaging, 2022, 2022.

[40] D. Moher, A. Liberati, J. Tetzlaff, D.G. Altman, T. Prisma Group, Preferred reporting items for systematic reviews and meta-analyses: the PRISMA statement Ann, Intern. Med. 151 (4) (2009) 264–269.

[41] M. Meher, S. Pradhan, S.R. Pradhan, Risk factors associated with hypertension in young adults: a systematic review, Cureus 15 (4) (2023) e37467, https://doi.org/10.7759/cureus.37467. PMID: 37187665; PMCID: PMC10181897.

[42] S. Singh, R. Shankar, G.P. Singh, Prevalence and associated risk factors of hypertension: a cross-sectional study in urban varanasi, Int. J. Hypertens. 2017 (2017) 5491838, https://doi.org/10.1155/2017/5491838. Epub 2017 Dec 3. PMID: 29348933; PMCID: PMC5733954.

[43] G.K. Paul, K.K. Karmoker, B. Sen, M.Z. Hussain, M.S. Hasan, M.K. Khan, Risk factors for hypertension in young adults of Bangladesh, Mymensingh Med. J. 29 (1) (2020 Jan) 43–47. PMID: 31915334.

[44] Nina P. Paynter, Nancy R. Cook, Brendan M. Everett, Howard D. Sesso, Julie E. Buring, Paul M. Ridker, Prediction of incident hypertension risk in women with currently normal blood pressure, Am. J. Med. 122 (Issue 5) (2009) 464–471, https://doi.org/10.1016/j.amjmed.2008.10.034.

[45] S. da, E.J. Luz, W.R. Schwartz, G. Camara-Chavez, D. Menotti, ECG-based heartbeat classification for arrhythmia detection: a survey, Comput. Methods Programs Biomed. 127 (2016) 144–164.

[46] G. Estrada, M. Luis, l.e. Mendoza, M. Sc, V. Molina, Relationship of blood pressure with the electrical signal of the heart using signal processing, Tecciencia 9 (17) (2014) 9–14.

[47] M. Sokolow, T.P. Lyon, The ventricular complex in left ventricular hypertrophy as obtained by unipolar precordial and limbs leads, Am. Heart J. 37 (1949) 161–186.

[48] Yongbo Liang, Guiyong Liu, Zhencheng Chen, Mohamed Elgendi, PPG-BP Database. Figshare. Dataset, 2017, https://doi.org/10.6084/m9.figshare.5459299.v2.

[49] M. Elgendi, R. Fletcher, Y. Liang, N. Howard, N. Lovell, D. Abbott, K. Lim, R. Ward, The use of photoplethysmography for assessing hypertension, Nat. Med. 2 (2019).

[50] Y. Liang, Z. Chen, R. Ward, M. Elgendi, Hypertension assessment using photoplethysmography: a risk stratification approach, J. Clin. Med. 8 (2018) 12.

[51] ui Wen Loh, Shuting Xu, Oliver Faust, Chui Ping Ooi, Prabal Datta Barua, Subrata Chakraborty, Ru-San Tan, Filippo Molinari, U. Rajendra Acharya, Application of photoplethysmography signals for healthcare systems: an in-depth review, Comput. Methods Progr. Biomed. 216 (2022) 106677, https://doi.org/10.1016/j.cmpb.2022.106677. ISSN 0169-2607.

[52] Task Force of the European Society of Cardiology and the North American Society of Pacing and Electrophysiology, Heart rate variability: standards of measurement, physiological interpretation, and clinical use, Circulation 93 (1996) 1043–1065.

[53] D. Liao, J. Cai, R.W. Barnes, H.A. Tyroler, P. Rautaharju, I. Holme, G. Heiss, Association of cardiac autonomic function and the development of hypertension: the ARIC Study, Am. J. Hypertens. 9 (1996) 1147–1156.

[54] J.P. Singh, M.G. Larson, H. Tsuji, J.C. Evans, C.J. O'Donnell, D. Levy, Reduced heart rate variability and new-onset hypertension: insights into pathogenesis of hypertension: the Framingham Heart Study, Hypertension 32 (1998) 293–297.

[55] Oliver Faust, Wanrong Hong, Hui Wen Loh, Shuting Xu, Ru-San Tan, Subrata Chakraborty, Prabal Datta Barua, U. Filippo Molinari, Rajendra Acharya, Heart rate variability for medical decision support systems: a review, Comput. Biol. Med. 145 (2022) 105407, https://doi.org/10.1016/j.compbiomed.2022.105407. ISSN 0010-4825.

[56] F. Liu, X. Zhou, Z. Wang, J. Cao, H. Wang, Y. Zhang, Unobtrusive mattress-based identification of hypertension by integrating classification and association Rule mining, Sensors 19 (2019) 1489, https://doi.org/10.3390/s19071489.

[57] H. Burger, J. Korsten, A. Noordergraaf, P. Ullersma, Physical basis of ballistocardiography. IV. The relative movement of subject and ballistocardiograph, Am. Heart J. 52 (1956) 653–673, https://doi.org/10.1016/0002-8703(56)90021-7.

[58] I. Starr, The relation of the ballistocardiogram to cardiac function, Am. J. Cardiol. 2 (1959) 737–747, https://doi.org/10.1016/0002-9149(58)90271-6.

[59] A. Knoop, Experimental Investigations on Ultra-low Frequency Displacement Ballistocardiography, National Aeronautics and Space Administration, Washington, DC, USA, 1965, pp. 1–107. NASA TT F-269; NASA Contractor Report.

[60] N. Miyai, M. Arita, K. Miyashita, I. Morioka, T. Shiraishi, I. Nishio, Blood pressure response to heart rate during exercise test and risk of future hypertension, Hypertension 39 (2002) 761–766, https://doi.org/10.1161/hy0302.105777.

[61] G. Thanassoulis, A. Lyass, E.J. Benjamin, M.G. Larson, J.A. Vita, D. Levy, et al., Relations of exercise blood pressure response to cardiovascular risk factors and vascular function in the framingham heart study, Circulation 125 (2012) 2836–2843, https://doi.org/10.1161/CIRCULATIONAHA.111.063933.

[62] M. Saeed, M. Villarroel, A.T. Reisner, G. Clifford, L. Lehman, G.B. Moody, T. Heldt, T.H. Kyaw, B.E. Moody, R.G. Mark, Multiparameter intelligent monitoring in intensive care II (MIMIC-II): a public-access ICU database, Crit. Care Med. 39 (5) (2011 May) 952–960, https://doi.org/10.1097/CCM.0b013e31820a92c6.

[63] C.L. Johnson, R. Paulose-Ram, C.L. Ogden, M.D. Carroll, D. Kruszan-Moran, S. M. Dohrmann, L.R. Curtin, National Health and Nutrition Examination Survey, Analytic guidelines, 2013, pp. 1999–2010.

[64] S. Cheol Seong, Y.Y. Kim, Y.H. Khang, J. Heon Park, H.J. Kang, H. Lee, S. Ae Shin, Data resource profile: the national health information database of the National Health Insurance Service in South Korea, Int. J. Epidemiol. 46 (3) (2017) 799–800.

[65] S. Garies, R. Birtwhistle, N. Drummond, J. Queenan, T. Williamson, Data resource profile: national electronic medical record data from the canadian primary care sentinel surveillance network (cpcssn), Int. J. Epidemiol. 46 (4) (2017) 1091–1092.

[66] Y. Luo, Y. Li, Y. Lu, S. Lin, X. Liu, The prediction of hypertension based on convolution neural network, in: 2018 IEEE 4th International Conference on Computer and Communications (ICCC), Chengdu, China, 2018, pp. 2122–2127, https://doi.org/10.1109/CompComm.2018.8780834.

[67] S. Montagna, M.F. Pengo, S. Ferretti, C. Borghi, C. Ferri, G. Grassi, G. Parati, Machine learning in hypertension detection: a study on World Hypertension Day data, J. Med. Syst. 47 (1) (2022) 1.

[68] M.M. Islam, M.J. Alam, M. Maniruzzaman, N.F. Ahmed, M.S. Ali, M.J. Rahman, D.C. Roy, Predicting the risk of hypertension using machine learning algorithms: a cross sectional study in Ethiopia, PLoS One 18 (8) (2023) e0289613.

[69] M.M. Baig, H.G. Hosseini, M. Lindén, Machine learning-based clinical decision support system for early diagnosis from real-time physiological data, in: 2016 IEEE Region 10 Conference (TENCON), IEEE, 2016, November, pp. 2943–2946.

[70] H.F. Golino, L.S.D.B. Amaral, S.F.P. Duarte, C.M.A. Gomes, T.D.J. Soares, L.A. D. Reis, J. Santos, Predicting increased blood pressure using machine learning, J. Obes. 2014 (2014) 637635, 12, https://doi.org/10.1155/2014/637635.

[71] D. LaFreniere, F. Zulkernine, D. Barber, K. Martin, Using machine learning to predict hypertension from a clinical dataset, in: 2016 IEEE Symposium Series on Computational Intelligence (SSCI), IEEE, 2016, December, pp. 1–7.

[72] H. He, Y. Bai, E.A. Garcia, S. Li, ADASYN: adaptive synthetic sampling approach for imbalanced learning, in: 2008 IEEE International Joint Conference on Neural Networks (IEEE World Congress on Computational Intelligence), IEEE, 2008, pp. 1322–1328.

[73] Y. Sakka, D. Qarashai, A. Altarawneh, Predicting hypertension using machine learning: a case study at petra university, Int. J. Adv. Comput. Sci. Appl. 14 (3) (2023).

[74] M. Fang, Y. Chen, R. Xue, H. Wang, N. Chakraborty, T. Su, Y. Dai, A hybrid machine learning approach for hypertension risk prediction, Neural Comput. Appl. 35 (20) (2023) 14487–14497.

[75] Y. Ren, H. Fei, X. Liang, D. Ji, M. Cheng, A hybrid neural network model for predicting kidney disease in hypertension patients based on electronic health records, BMC Med. Inf. Decis. Making 19 (2019) 131–138.

[76] I. Elizabeth Kumar, Venkatasubramanian Suresh, Carlos Scheidegger, Sorelle Friedler, Problems with shapley-value-based explanations as feature importance measures, Proceedings of the 37th International Conference on Machine Learning 119 (July 2020) 5491–5500.

[77] L.C. Shih, Y.C. Wang, M.H. Hung, H. Cheng, Y.C. Shiao, Y.H. Tseng, J.W. Chen, Prediction of white-coat hypertension and white-coat uncontrolled hypertension using machine learning algorithm, European Heart Journal-Digital Health 3 (4) (2022) 559–569.

[78] https://archive.physionet.org/mimic2/(accessed on 15/November/2023).

[79] https://physionet.org/content/mimiciii/1.4/(accessed on 15/November/2023).

[80] https://physionet.org/content/mimiciv/2.2/(accessed on 15/November/2023).

[81] https://eicu-crd.mit.edu/(accessed on 15/November/2023).

[82] https://physionet.org/content/mimic3wdb/1.0/(accessed on 15/November/2023).

[83] https://physionet.org/content/shareedb/1.0.0/(accessed on 15/November/2023).

[84] Y.H. Tanc, M. Ozturk, Hypertension classification using PPG signals, in: 2022 Medical Technologies Congress (TIPTEKNO), IEEE, 2022, pp. 1–4.

[85] C. Szegedy, W. Liu, Y. Jia, P. Sermanet, S. Reed, D. Anguelov, A. Rabinovich, Going deeper with convolutions, in: Proceedings of the IEEE Conference on Computer Vision and Pattern Recognition, 2015, pp. 1–9.

[86] S.S. Mousavi, M. Firouzmand, M. Charmi, M. Hemmati, M. Moghadam, Y. Ghorbani, Blood pressure estimation from appropriate and inappropriate PPG signals using A whole-based method, Biomed. Signal Process Control 47 (2019) 196–206.

[87] M. Khan, B.K. Singh, N. Nirala, M.T. Hasan, M. Nasiruddin, Multi-domain feature-based expert diagnostic system for detection of hypertension using photoplethysmogram signal, International Journal of Intelligent Systems and Applications in Engineering 10 (4) (2022) 424–433.

[88] V.R. Nafisi, M. Shahabi, Intradialytic hypotension related episodes identification based on the most effective features of photoplethysmography signal, Comput. Methods Progr. Biomed. 157 (2018) 1–9.

[89] E. Mejía-Mejía, J.M. May, M. Elgendi, P.A. Kyriacou, Classification of blood pressure in critically ill patients using photoplethysmography and machine learning, Comput. Methods Progr. Biomed. 208 (2021) 106222.

[90] E. Martinez-Ríos, L. Montesinos, M. Alfaro-Ponce, A machine learning approach for hypertension detection based on photoplethysmography and clinical data, Comput. Biol. Med. 145 (2022) 105479.

[91] A.D. Junior, S. Murali, F. Rincon, D. Atienza, Methods for reliable estimation of pulse transit time and blood pressure variations using smartphone sensors, Microprocess. Microsyst. 46 (2016) 84–95.

[92] M. Rong, K. Li, A multi-type features fusion neural network for blood pressure prediction based on photoplethysmography, Biomed. Signal Process Control 68 (2021) 102772.

[93] B.K. Singh, N. Nirala, Expert diagnostic system for detection of hypertension and diabetes mellitus using discrete wavelet decomposition of photoplethysmogram signal and machine learning technique, Medicine in Novel Technology and Devices 19 (2023) 100251.

[94] M.U. Khan, S. Aziz, T. Akram, F. Amjad, K. Iqtidar, Y. Nam, M.A. Khan, Expert hypertension detection system featuring pulse plethysmograph signals and hybrid feature selection and reduction scheme, Sensors 21 (1) (2021) 247.

[95] L. Evdochim, D. Dobrescu, S. Halichidis, L. Dobrescu, S. Stanciu, Hypertension detection based on photoplethysmography signal morphology and machine learning techniques, Appl. Sci. 12 (16) (2022) 8380.

[96] H. Tjahjadi, K. Ramli, Noninvasive blood pressure classification based on photoplethysmography using k-nearest neighbors algorithm: a feasibility study, Information 11 (2) (2020) 93.

[97] L.P. Yao, W.Z. Liu, Hypertension assessment based on feature extraction using a photoplethysmography signal and its derivatives, Physiol. Meas. 42 (6) (2021) 065001.

[98] S. Gupta, A. Singh, A. Sharma, R.K. Tripathy, Higher order derivative-based integrated model for cuff-less blood pressure estimation and stratification using PPG signals, IEEE Sensor. J. 22 (22) (2022) 22030–22039.

[99] P. Ranjan, A. Kumar, R. Kumar, M. Sameer, B. Gupta, Automated detection of blood pressure using CNN, in: 2022 IEEE Delhi Section Conference (DELCON), IEEE, 2022, pp. 1–5.

[100] G. Sannino, I. De Falco, G. De Pietro, Non-invasive risk stratification of hypertension: a systematic comparison of machine learning algorithms, J. Sens. Actuator Netw. 9 (3) (2020) 34.

[101] N.F. Ali, M. Atef, An efficient hybrid LSTM-ANN joint classification-regression model for PPG based blood pressure monitoring, Biomed. Signal Process Control 84 (2023) 104782.

[102] N.I. Echeverría, A.G. Scandurra, C.M. Acosta, G.J. Meschino, F.S. Sipmann, G. Tusman, Photoplethysmography waveform analysis for classification of vascular tone and arterial blood pressure: study based on neural networks, Rev. Esp. Anestesiol. Reanim. 70 (4) (2023) 209–217.

[103] A. Rashkovska, M. Depolli, I. Tomašić, V. Avbelj, R. Trobec, Medical-grade ECG sensor for long-term monitoring, Sensors 20 (6) (2020 Mar 18) 1695, https://doi.org/10.3390/s20061695. PMID: 32197444; PMCID: PMC7146736.).

[104] D.C.K. Soh, E.Y.K. Ng, V. Jahmunah, S.L. Oh, T.R. San, U.R. Acharya, A computational intelligence tool for the detection of hypertension using empirical mode decomposition, Comput. Biol. Med. 118 (2020) 103630.

[105] K.S. Parmar, A. Kumar, U. Kalita, ECG signal based automated hypertension detection using fourier decomposition method and cosine modulated filter banks, Biomed. Signal Process Control 76 (2022) 103629.

[106] J.S. Rajput, M. Sharma, R. San Tan, U.R. Acharya, Automated detection of severity of hypertension ECG signals using an optimal bi-orthogonal wavelet filter bank, Comput. Biol. Med. 123 (2020) 103924.

[107] J.S. Rajput, M. Sharma, U.R. Acharya, Hypertension diagnosis index for discrimination of high-risk hypertension ECG signals using optimal orthogonal wavelet filter bank, Int. J. Environ. Res. Publ. Health 16 (21) (2019) 4068.

[108] L. Alkukhun, X.F. Wang, M.K. Ahmed, M. Baumgartner, M.M. Budev, R.A. Dweik, A.R. Tonelli, Non-invasive screening for pulmonary hypertension in idiopathic pulmonary fibrosis, Respir. Med. 117 (2016) 65–72.

[109] M.E. Hesar, N.S. Seyedsadrkhani, D. Khan, A. Naghashian, M. Piekarski, H. Gall, S. Ingebrandt, AI-enabled epidermal electronic system to automatically monitor a prognostic parameter for hypertension with a smartphone, Biosens. Bioelectron. 241 (2023) 115693.

[110] J. Esmaelpoor, M.H. Moradi, A. Kadkhodamohammadi, A multistage deep neural network model for blood pressure estimation using photoplethysmogram signals, Comput. Biol. Med. 120 (2020) 103719.

[111] P. Jain, P. Gajbhiye, R.K. Tripathy, U.R. Acharya, A two-stage deep CNN architecture for the classification of low-risk and high-risk hypertension classes using multi-lead ECG signals, Inform. Med. Unlocked 21 (2020) 100479.

[112] M.M. Islam, R. Shamsuddin, Machine learning to promote health management through lifestyle changes for hypertension patients, Array 12 (2021) 100090.

[113] C. Chen, H.Y. Zhao, S.H. Zheng, R.A. Ramachandra, X. He, Y.H. Zhang, V. K. Sudarshan, Interpretable hybrid model for an automated patient-wise categorization of hypertensive and normotensive electrocardiogram signals, Computer Methods and Programs in Biomedicine Update 3 (2023) 100097.

[114] T. Habineza, A.H. Ribeiro, D. Gedon, J.A. Behar, A.L.P. Ribeiro, T.B. Schön, End-to-end risk prediction of atrial fibrillation from the 12-Lead ECG by deep neural networks, J. Electrocardiol. 81 (2023) 193–200.

[115] J.S. Haimovich, N. Diamant, S. Khurshid, P. Di Achille, C. Reeder, S. Friedman, S. A. Lubitz, Artificial intelligence–enabled classification of hypertrophic heart diseases using electrocardiograms, Cardiovascular Digital Health Journal 4 (2) (2023) 48–59.

[116] N. Hirota, S. Suzuki, J. Motogi, T. Umemoto, H. Nakai, W. Matsuzawa, T. Yamashita, Identification of patients with dilated phase of hypertrophic cardiomyopathy using a convolutional neural network applied to multiple, dual, and single lead electrocardiograms, IJC Heart & Vasculature 46 (2023) 101211.

[117] S.R. Rooney, R. Kaufman, R. Murugan, K.B. Kashani, M.R. Pinsky, S. Al-Zaiti, J. K. Miller, Forecasting imminent atrial fibrillation in long-term electrocardiogram recordings, J. Electrocardiol. 81 (2023) 111–116.

[118] M.A. Aras, S. Abreau, H. Mills, L. Radhakrishnan, L. Klein, N. Mantri, G.H. Tison, Electrocardiogram detection of pulmonary hypertension using deep learning, J. Card. Fail. 29 (7) (2023 Jul) 1017–1028.

[119] F. Miao, B. Wen, Z. Hu, G. Fortino, X.P. Wang, Z.D. Liu, Y. Li, Continuous blood pressure measurement from one-channel electrocardiogram signal using deep-learning techniques, Artif. Intell. Med. 108 (2020) 101919.

[120] S. Baker, W. Xiang, I. Atkinson, A hybrid neural network for continuous and non-invasive estimation of blood pressure from raw electrocardiogram and photoplethysmogram waveforms, Comput. Methods Progr. Biomed. 207 (2021) 106191.

[121] N. Natarajan, A. Balakrishnan, K. Ukkirapandian, A study on analysis of Heart Rate Variability in hypertensive individuals, Int. J. Biomed. Adv. Res. 5 (2014) 109.

[122] M.G. Poddar, V. Kumar, Y.P. Sharma, Linear-nonlinear heart rate variability analysis and SVM based classification of normal and hypertensive subjects, J. Electrocardiol. 46 (4) (2013) e25.

[123] M.G. Poddar, A.C. Birajdar, J. Virmani, Automated classification of hypertension and coronary artery disease patients by PNN, KNN, and SVM classifiers using HRV analysis, in: Machine Learning in Bio-Signal Analysis and Diagnostic Imaging, Academic Press, 2019, pp. 99–125.

[124] B.K. Koichubekov, M.A. Sorokina, Y.M. Laryushina, L.G. Turgunova, I. V. Korshukov, Nonlinear analyses of heart rate variability in hypertension, Ann. Cardiol. Angeiol 67 (3) (2018, June) 174–179. Elsevier Masson.

[125] V.S. Kublanov, A.Y. Dolganov, D. Belo, H. Gamboa, Comparison of machine learning methods for the arterial hypertension diagnostics, Appl. Bionics Biomechanics 2017 (2017) 5985479, https://doi.org/10.1155/2017/5985479.

[126] H. Ni, Y. Wang, G. Xu, Z. Shao, W. Zhang, X. Zhou, Multiscale fine-grained heart rate variability analysis for recognizing the severity of hypertension, Comput. Math. Methods Med. 2019 (2019) 9. https://doi.org/10.1155/2019/4936179, 4936179.

[127] Y. Song, H. Ni, X. Zhou, W. Zhao, T. Wang, Extracting features for cardiovascular disease classification based on ballistocardiography, in: 2015 IEEE 12th Intl Conf on Ubiquitous Intelligence and Computing and 2015 IEEE 12th Intl Conf on Autonomic and Trusted Computing and 2015 IEEE 15th Intl Conf on Scalable Computing and Communications and its Associated Workshops (UIC-ATC-ScalCom), IEEE, 2015, August, pp. 1230–1235.

[128] S.T. Ozcelik, H. Uyanık, E. Deniz, A. Sengur, Automated hypertension detection using ConvMixer and Spectrogram techniques with ballistocardiograph signals, Diagnostics 13 (2) (2023) 182.

[129] K. Gupta, V. Bajaj, I.A. Ansari, A support system for automatic classification of hypertension using BCG signals, Expert Syst. Appl. 214 (2023) 119058.

[130] J.S. Rajput, M. Sharma, D. Kumbhani, U.R. Acharya, Automated detection of hypertension using wavelet transform and nonlinear techniques with ballistocardiogram signals, Inform. Med. Unlocked 26 (2021) 100736.

[131] J.S. Rajput, M. Sharma, T.S. Kumar, U.R. Acharya, Automated detection of hypertension using continuous wavelet transform and a deep neural network with Ballistocardiography signals, Int. J. Environ. Res. Publ. Health 19 (7) (2022) 4014.

[132] K. Gupta, V. Bajaj, I.A. Ansari, U.R. Acharya, Hyp-Net: automated detection of hypertension using deep convolutional neural network and Gabor transform techniques with ballistocardiogram signals, Biocybern. Biomed. Eng. 42 (3) (2022) 784–796.

[133] Yasna Forghani, Behnam Hamid, Maryam Shojaeifard, Hypertrophic cardiomyopathy (HCM) and hypertensive heart disease (HHD) diagnosis using echocardiography and electrocardiography, Comput. Methods Biomech. Biomed. Eng.: Imaging & Visualization 9 (6) (2021) 565–573, https://doi.org/10.1080/21681163.2021.1894486.

[134] J. Cano, V. Bertomeu-González, L. Fácila, R. Zangróniz, R. Alcaraz, J.J. Rieta, Hypertension risk assessment from photoplethysmographic recordings using deep learning classifiers, in: 2021 Computing in Cardiology (CinC), IEEE, 2021, September, pp. 1–4 (vol. 48.

[135] S. Mahmud, N. Ibtehaz, A. Khandakar, M.S. Rahman, A.J. Gonzales, T. Rahman, M.E. Chowdhury, NABNet: a nested attention-guided BiConvLSTM network for a robust prediction of blood pressure components from reconstructed arterial blood pressure waveforms using PPG and ECG signals, Biomed. Signal Process Control 79 (2023) 104247.

[136] W. Long, X. Wang, BPNet: a multi-modal fusion neural network for blood pressure estimation using ECG and PPG, Biomed. Signal Process Control 86 (2023) 105287.

[137] Y. Liang, Z. Chen, R. Ward, M. Elgendi, Photoplethysmography and deep learning: enhancing hypertension risk stratification, Biosensors 8 (4) (2018) 101.

[138] X.L. Zou, Y. Ren, D.Y. Feng, X.Q. He, Y.F. Guo, H.L. Yang, T.T. Zhang, A promising approach for screening pulmonary hypertension based on frontal chest radiographs using deep learning: a retrospective study, PLoS One 15 (7) (2020) e0236378.

[139] Y. Qiu, D. Liu, G. Yang, D. Qi, Y. Lu, Q. He, J. Shuai, Cuffless blood pressure estimation based on composite neural network and graphics information, Biomed. Signal Process Control 70 (2021) 103001.

[140] K.C. Lan, P. Raknim, W.F. Kao, J.H. Huang, Toward hypertension prediction based on PPG-derived HRV signals: a feasibility study, J. Med. Syst. 42 (2018) 1–7.
[141] A.E. Burchell, J.C. Rodrigues, M. Charalambos, L.E. Ratcliffe, E.C. Hart, J. F. Paton, A. Baumbach, N.E. Manghat, A.K. Nightingale, Comprehensive first-line magnetic resonance imaging in hypertension: experience from a single-center tertiary referral clinic, J. Clin. Hypertens. 19 (1) (2017) 13–22, https://doi.org/10.1111/jch.12920. Epub 2016 Oct 19. PMID: 27759186; PMCID: PMC8031106.
[142] D. Liao, L. Cooper, J. Cai, J.F. Toole, N.R. Bryan, R.G. Hutchinson, H.A. Tyroler, Presence and severity of cerebral white matter lesions and hypertension, its treatment, and its control. The ARIC Study. Atherosclerosis Risk in Communities Study, Stroke 27 (1996) 2262–2270.
[143] W.T. Longstreth Jr., T.A. Manolio, A. Arnold, G.L. Burke, N. Bryan, C.A. Jungreis, P.L. Enright, D. O'Leary, L. Fried, Clinical correlates of white matter findings on cranial magnetic resonance imaging of 3301 elderly people. The Cardiovascular Health Study, Stroke 27 (1996) 1274–1282.
[144] J.T. O'Brien, T. Erkinjuntti, B. Reisberg, G. Roman, T. Sawada, L. Pantoni, J. V. Bowler, C. Ballard, C. DeCarli, P.B. Gorelick, K. Rockwood, A. Burns, S. Gauthier, S.T. DeKosky, Vascular cognitive impairment, Lancet Neurol. 2 (2003) 89–98.
[145] S.E. Vermeer, M. Hollander, E.J. Van Dijk, A. Hofman, P.J. Koudstaal, M. M. Breteler, Silent brain infarcts and white matter lesions increase stroke risk in the general population: the Rotterdam scan study, Stroke 34 (2003) 1126–1129.
[146] S.E. Vermeer, N.D. Prins, T. den Heijer, A. Hofman, P.J. Koudstaal, M.M. Breteler, Silent brain infarcts and the risk of dementia and cognitive decline, N. Engl. J. Med. 348 (2003) 1215–1222.
[147] D. Levy, R.J. Garrison, D.D. Savage, W.B. Kannel, W.P. Castelli, Prognostic implications of echocardiographically determined left ventricular mass in the Framingham Heart Study, N. Engl. J. Med. 322 (1990) 1561–1566.
[148] K. Wachtell, B. Dahlℓof, J. Rokkedal, V. Papademetriou, M.S. Nieminen, G. Smith, et al., Change of left ventricular geometric pattern after 1 year of antihypertensive treatment: the Losartan Intervention for Endpoint reduction in hypertension (LIFE) study, Am. Heart J. 144 (2002) 1057–1064.
[149] J. Zhou, M. Du, S. Chang, Z. Chen, Artificial intelligence in echocardiography: detection, functional evaluation, and disease diagnosis, Cardiovasc. Ultrasound 19 (2021) 29.
[150] R.M. Lang, L.P. Badano, W. Tsang, D.H. Adams, E. Agricola, T. Buck, et al., EAE/ASE recommendations for image acquisition and display using three dimensional echocardiography, J. Am. Soc. Echocardiogr. 25 (2012) 3–46.
[151] S.F. Nagueh, O.A. Smiseth, C.P. Appleton, B.F. Byrd 3rd, H. Dokainish, T. Edvardsen, et al., Recommendations for the evaluation of left ventricular diastolic function by echocardiography: an update from the American society of echocardiography and the European association of cardiovascular imaging, Eur Heart J Cardiovasc Imaging 17 (2016) 1321–1360.
[152] M.L. Muiesan, M. Salvetti, C. Monteduro, B. Bonzi, A. Paini, S. Viola, et al., Left ventricular concentric geometry during treatment adversely affects cardiovascular prognosis in hypertensive patients, Hypertension 43 (2004) 731–738 (Dallas, Tex: 1979).
[153] S. Garg, J.A. de Lemos, C. Ayers, M.G. Khouri, A. Pandey, J.D. Berry, et al., Association of a 4-tiered classification of LV hypertrophy with adverse CV outcomes in the general population, JACC Cardiovasc Imaging 8 (2015) 1034–1041.
[154] D.J. Breslin, R.W. Gifford Jr., J.F. Fairbairn 2nd, T.P. Kearns, Prognostic importance of ophthalmoscopic findings in essential hypertension, JAMA 195 (1966) 335–338.
[155] T. Sairenchi, H. Iso, K. Yamagishi, F. Irie, Y. Okubo, J. Gunji, et al., Mild retinopathy is a risk factor for cardiovascular mortality in Japanese with and without hypertension: the Ibaraki Prefectural Health Study, Circulation 124 (2011) 2502–2511.
[156] B.K. Triwijoyo, W. Budiharto, E. Abdurachman, The classification of hypertensive retinopathy using convolutional neural network, Procedia Comput. Sci. 116 (2017) 166–173.
[157] E.A. Warnert, J.C. Rodrigues, A.E. Burchell, S. Neumann, L.E. Ratcliffe, N. E. Manghat, A.D. Harris, Z. Adams, A.K. Nightingale, R.G. Wise, J.F. Paton, E. C. Hart, Is high blood pressure self-protection for the brain? Circ. Res. 119 (12) (2016 Dec 9) e140–e151, https://doi.org/10.1161/CIRCRESAHA.116.309493. Epub 2016 Sep 26. PMID: 27672161.
[158] H. Kandil, A. Soliman, N. Elsaid, A. Saied, N.S. Alghamdi, A. Mahmoud, A. El-Baz, Studying the role of cerebrovascular changes in different compartments in human brains in hypertension prediction, Appl. Sci. 12 (9) (2022) 4291.
[159] H. Kandil, et al., A CAD system for the early prediction of hypertension based on changes in cerebral vasculature, in: 2019 IEEE International Conference on Imaging Systems and Techniques (IST), United Arab Emirates, Abu Dhabi, 2019, pp. 1–5, https://doi.org/10.1109/IST48021.2019.9010179.
[160] H. Kandil, A. Soliman, F. Taher, M. Ghazal, M. Hadi, G. Giridharan, A. El-Baz, A cad system for the early prediction of hypertension based on changes in cerebral vasculature, in: 2019 IEEE International Conference on Imaging Systems and Techniques (IST), IEEE, 2019, December, pp. 1–5.
[161] F. Taher, A. Soliman, H. Kandil, A. Mahmoud, A. Shalaby, G. Gimel'farb, A. El-Baz, Precise cerebrovascular segmentation, in: 2020 IEEE International Conference on Image Processing (ICIP), IEEE, 2020, October, pp. 394–397.
[162] H. Kandil, A. Soliman, M. Ghazal, A. Mahmoud, A. Shalaby, R. Keynton, A. El-Baz, A novel framework for early detection of hypertension using magnetic resonance angiography, Sci. Rep. 9 (1) (2019) 11105.
[163] H. Kandil, A. Soliman, N.S. Alghamdi, J.R. Jennings, A. El-Baz, Using mean arterial pressure in hypertension diagnosis versus using either systolic or diastolic blood pressure measurements, Biomedicines 11 (3) (2023) 849.
[164] S. Li, L. Zhao, B. Zhang, Y. Yuan, H. Cao, Z. Yu, Ultrasound cardiogram-based diagnosis of cardiac hypertrophy from hypertension and analysis of its relationship with expression of autophagy-related protein, Ann. Palliat. Med. 11 (2) (2022) 684–694.
[165] A. Gudigar, U. Raghavendra, T. Devasia, K. Nayak, S.M. Danish, G. Kamath, U. R. Acharya, Global weighted LBP-based entropy features for the assessment of pulmonary hypertension, Pattern Recogn. Lett. 125 (2019) 35–41.
[166] A. Leha, K. Hellenkamp, B. Unsöld, S. Mushemi-Blake, A.M. Shah, G. Hasenfuß, T. Seidler, A machine learning approach for the prediction of pulmonary hypertension, PLoS One 14 (10) (2019) e0224453.
[167] G.P. Diller, M.L. Benesch Vidal, A. Kempny, K. Kubota, W. Li, K. Dimopoulos, M. A. Gatzoulis, A framework of deep learning networks provides expert-level accuracy for the detection and prognostication of pulmonary arterial hypertension, European Heart Journal-Cardiovascular Imaging 23 (11) (2022) 1447–1456.
[168] H. Ragnarsdottir, L. Manduchi, H. Michel, F. Laumer, S. Wellmann, E. Ozkan, J. E. Vogt, Interpretable prediction of pulmonary hypertension in newborns using echocardiograms, in: DAGM German Conference on Pattern Recognition, Springer International Publishing, Cham, 2022, September, pp. 529–542.
[169] J. Chen, X. Zhang, J. Yuan, R. Shao, C. Gan, Q. Ji, H. Zhu, Weakly supervised video-based cardiac detection for hypertensive cardiomyopathy, BMC Med. Imag. 23 (1) (2023) 163.
[170] Z. Liao, K. Liu, S. Ding, Q. Zhao, Y. Jiang, L. Wang, H. Fei, Automatic echocardiographic evaluation of the probability of pulmonary hypertension using machine learning, Pulm. Circ. 13 (3) (2023) e12272.
[171] K. Kusunose, Y. Hirata, N. Yamaguchi, Y. Kosaka, T. Tsuji, J.I. Kotoku, M. Sata, Deep learning for detection of exercise-induced pulmonary hypertension using chest X-ray images, Frontiers in Cardiovascular Medicine 9 (2022) 891703.
[172] L. Zhang, M. Yuan, Z. An, X. Zhao, H. Wu, et al., Prediction of hypertension, hyperglycemia and dyslipidemia from retinal fundus photographs via deep learning: a cross-sectional study of chronic diseases in central China, PLoS One 15 (5) (2020) e0233166, https://doi.org/10.1371/journal.pone.0233166.
[173] S. Morales, V. Naranjo, A. Navea, M. Alcañiz, Computer-aided diagnosis software for hypertensive risk determination through fundus image processing, IEEE Journal of Biomedical and Health Informatics 18 (6) (Nov. 2014) 1757–1763, https://doi.org/10.1109/JBHI.2014.2337960.
[174] G. Robertson, A. Fleming, M.C. Williams, E. Trucco, N. Quinn, R. Hogg, G. J. McKay, F. Kee, I. Young, E. Pellegrini, D.E. Newby, E.J.R. van Beek, T. Peto, B. Dhillon, J. van Hemert, T.J. MacGillivray, Northern Ireland Cohort of Longitudinal Ageing. Association between hypertension and retinal vascular features in ultra-widefield fundus imaging, Open Heart 7 (1) (2020) e001124, https://doi.org/10.1136/openhrt-2019-001124. PMID: 32076560; PMCID: PMC6999694.
[175] J. Staal, M.D. Abramoff, M. Niemeijer, M.A. Viergever, B. van Ginneken, Ridge-based vessel segmentation in color images of the retina, IEEE Trans. Med. Imag. 23 (4) (2004) 501–509, https://doi.org/10.1109/TMI.2004.825627.
[176] S. Holm, G. Russell, V. Nourrit, N. McLoughlin, DR HAGIS-a fundus image database for the automatic extraction of retinal surface vessels from diabetic patients, J. Med. Imaging 4 (1) (2017 Jan) 014503, https://doi.org/10.1117/1.JMI.4.1.014503. Epub 2017 Feb 9. PMID: 28217714; PMCID: PMC5299858.
[177] T. Kauppi, V. Kalesnykiene, J. Kamarainen, L. Lensu, I. Sorri, DIARETDB0 : evaluation database and methodology for diabetic retinopathy algorithms, in: Mach. Vis. Pattern Recognit. Res. Group, Lappeenranta Univ. Technol, Finland, 2006, pp. 1–17 [Online], http://www.siue.edu/~sumbaug/RetinalProjectPapers/Diabetic Retinopathy Image Database Information.pdf.
[178] T. Kauppi, V. Kalesnykiene, J.K. Kamarainen, L. Lensu, I. Sorri, A. Raninen, J. Pietilä, The diaretdb1 diabetic retinopathy database and evaluation protocol, in: The 17th British Machine Vision Conference (BMVC), 2007, pp. 1–10, 1.
[179] Q. Abbas, M.E.A. DenseHyper Ibrahim, An automatic recognition system for detection of hypertensive retinopathy using dense features transform and deep-residual learning, Multimed. Tool. Appl. 79 (2020) 31595–31623, https://doi.org/10.1007/s11042-020-09630-x.
[180] U. Bhimavarapu, Automatic detection of hypertensive retinopathy using improved fuzzy clustering and novel loss function, Multimed. Tool. Appl. 82 (2023) 30107–30123, https://doi.org/10.1007/s11042-023-15044-2.
[181] M.Z. Sajid, I. Qureshi, Q. Abbas, M. Albathan, K. Shaheed, A. Youssef, S. Ferdous, A. Hussain, Mobile-HR: an ophthalmologic-based classification system for diagnosis of hypertensive retinopathy using optimized MobileNet architecture, Diagnostics 13 (8) (2023) 1439, https://doi.org/10.3390/diagnostics13081439.
[182] E. Mishima, J. Hashimoto, Y. Akiyama, H. Shima, K. Seiji, K. Takase, T. Abe, S. Ito, Impact of small renal ischemia in hypertension development: renovascular hypertension caused by small branch artery stenosis, J. Clin. Hypertens. 18 (3) (2016 Mar) 248–249, https://doi.org/10.1111/jch.12661. Epub 2015 Aug 21. PMID: 26293888; PMCID: PMC8031562.
[183] R. Parikh, A. Mathai, S. Parikh, G.C. Sekhar, R. Thomas, Understanding and using sensitivity, specificity and predictive values, Indian J. Ophthalmol. 56 (1) (2008) 45.
[184] S.K. Khare, V. Blanes-Vidal, E.S. Nadimi, U.R. Acharya, Emotion Recognition and Artificial Intelligence: A Systematic Review (2014–2023) and Research Recommendations, Information Fusion, 2023 102019.

[185] M. Salvi, H.W. Loh, S. Seoni, P.D. Barua, S. García, F. Molinari, U.R. Acharya, Multi-Modality Approaches for Medical Support Systems: A Systematic Review of the Last Decade, Information Fusion, 2023 102134.
[186] V. Jahmunah, J.E.W. Koh, V.K. Sudarshan, U. Raghavendra, A. Gudigar, S.L. Oh, U.R. Acharya, Endoscopy, Video Capsule Endoscopy, and Biopsy for Automated Celiac Disease Detection: A Review, Biocybernetics and Biomedical Engineering, 2022.
[187] V.K. Sudarshan, U. Raghavendra, A. Gudigar, E.J. Ciaccio, A. Vijayananthan, R. Sahathevan, U.R. Acharya, Assessment of CT for the categorization of hemorrhagic stroke (HS) and cerebral amyloid angiopathy hemorrhage (CAAH): a review, Biocybern. Biomed. Eng. 42 (3) (2022) 888–901.
[188] A. Gudigar, U. Raghavendra, S. Nayak, C.P. Ooi, W.Y. Chan, M.R. Gangavarapu, U.R. Acharya, Role of artificial intelligence in COVID-19 detection, Sensors 21 (23) (2021) 8045.
[189] S.K. Khare, S. March, P.D. Barua, V.M. Gadre, U.R. Acharya, Application of Data Fusion for Automated Detection of Children with Developmental and Mental Disorders: A Systematic Review of the Last Decade, Information Fusion, 2023 101898.
[190] T. Fawcett, ROC graphs: notes and practical considerations for researchers, Mach. Learn. 31 (1) (2004) 1–38.
[191] S.M.S. Islam, A. Talukder, M.A. Awal, M.M.U. Siddiqui, M.M. Ahamad, B. Ahammed, R. Maddison, Machine learning approaches for predicting hypertension and its associated factors using population-level data from three south asian countries, Frontiers in Cardiovascular Medicine 9 (2022) 839379.
[192] R. Kurniawan, B. Utomo, K.N. Siregar, K. Ramli, B. Besral, R.J. Suhatril, O. A. Pratiwi, Hypertension prediction using machine learning algorithm among Indonesian adults, IAES Int. J. Artif. Intell. 12 (2) (2023) 776.
[193] J.A. Orozco Torres, A. Medina Santiago, J.M. Villegas Izaguirre, M. Amador García, A. Delgado Hernández, Hypertension diagnosis with backpropagation neural networks for sustainability in public health, Sensors 22 (14) (2022) 5272.
[194] K. Gupta, N. Jiwani, N. Afreen, Blood pressure detection using CNN-LSTM model, in: 2022 IEEE 11th International Conference on Communication Systems and Network Technologies (CSNT), IEEE, 2022, April, pp. 262–366.
[195] E.S.A. El-Dahshan, M.M. Bassiouni, S.K. Khare, R.S. Tan, U.R. Acharya, ExHyptNet: an explainable diagnosis of hypertension using EfficientNet with PPG signals, Expert Syst. Appl. (2023) 122388.
[196] J. Wu, H. Liang, C. Ding, X. Huang, J. Huang, Q. Peng, Improving the accuracy in classification of blood pressure from photoplethysmography using continuous wavelet transform and deep learning, Int. J. Hypertens. (2021) 2021.
[197] P. Amorim, T. Moraes, D. Fazanaro, J. Silva, H. Pedrini, Shearlet and contourlet transforms for analysis of electrocardiogram signals, Comput. Methods Progr. Biomed. 161 (2018) 125–132.
[198] W.Y. Ko, K.C. Siontis, Z.I. Attia, R.E. Carter, S. Kapa, S.R. Ommen, P. A. Noseworthy, Detection of hypertrophic cardiomyopathy using a convolutional neural network-enabled electrocardiogram, J. Am. Coll. Cardiol. 75 (7) (2020) 722–733.
[199] L. Zhang, Z. Ji, F. Yang, G. Chen, Noninvasive continuous blood pressure estimation with fewer parameters based on RA-ReliefF feature selection and MPGA-BPN models, Biomed. Signal Process Control 84 (2023) 104757.
[200] P. Melillo, R. Izzo, A. Orrico, P. Scala, M. Attanasio, M. Mirra, L. Pecchia, Automatic prediction of cardiovascular and cerebrovascular events using heart rate variability analysis, PLoS One 10 (3) (2015) e0118504.
[201] H. Ni, S. Cho, J. Mankoff, J. Yang, A.K. Dey, Automated recognition of hypertension through overnight continuous HRV monitoring, J. Ambient Intell. Hum. Comput. 9 (2018) 2011–2023.
[202] S. Si, C. Sun, H. Wang, H. Wu, L. Chen, Y. Xia, J. Yang, Unconstrained blood pressure monitoring based on a neural network–assisted multistage pressure textile sensor, Nano Energy 115 (2023) 108730.
[203] A. Ghosh, J.M.M. Torres, M. Danieli, G. Riccardi, Detection of essential hypertension with physiological signals from wearable devices, in: 2015 37th Annual International Conference of the IEEE Engineering in Medicine and Biology Society (EMBC), IEEE, 2015, August, pp. 8095–8098.
[204] B. Huang, W. Chen, C.L. Lin, C.F. Juang, J. Wang, MLP-BP: a novel framework for cuffless blood pressure measurement with PPG and ECG signals based on MLP-Mixer neural networks, Biomed. Signal Process Control 73 (2022) 103404.
[205] I. Sharifi, S. Goudarzi, M.B. Khodabakhshi, A novel dynamical approach in continuous cuffless blood pressure estimation based on ECG and PPG signals, Artif. Intell. Med. 97 (2019) 143–151.
[206] G. Thambiraj, U. Gandhi, U. Mangalanathan, V.J.M. Jose, M. Anand, Investigation on the effect of Womersley number, ECG and PPG features for cuff less blood pressure estimation using machine learning, Biomed. Signal Process Control 60 (2020) 101942.
[207] A. Gudigar, et al., Directional-Guided motion sensitive descriptor for automated detection of hypertension using ultrasound images, IEEE Access 12 (2024) 3659–3671, https://doi.org/10.1109/ACCESS.2023.3349090.
[208] Massimo Salvi, Hui Wen Loh, Silvia Seoni, Prabal Datta Barua, Salvador García, U. Filippo Molinari, Rajendra Acharya, Multi-modality approaches for medical support systems: a systematic review of the last decade, Inf. Fusion 103 (2024) 102134, https://doi.org/10.1016/j.inffus.2023.102134. ISSN 1566-2535.
[209] A. Dosovitskiy, L. Beyer, A. Kolesnikov, D. Weissenborn, X. Zhai, T. Unterthiner, Transformers for Image Recognition at Scale, 2020, 2010.11929.
[210] M. Abdar, F. Pourpanah, S. Hussain, D. Rezazadegan, L. Liu, M. Ghavamzadeh, S. Nahavandi, A review of uncertainty quantification in deep learning: techniques, applications and challenges, Inf. Fusion 76 (2021) 243–297.
[211] Silvia Seoni, Vicnesh Jahmunah, Massimo Salvi, Prabal Datta Barua, Filippo Molinari, U. Rajendra Acharya, Application of uncertainty quantification to artificial intelligence in healthcare: a review of last decade (2013–2023), Comput. Biol. Med. 165 (2023) 107441, https://doi.org/10.1016/j.compbiomed.2023.107441. ISSN 0010-4825.
[212] A. Saranya, R. Subhashini, A systematic review of Explainable Artificial Intelligence models and applications: recent developments and future trends, Decision analytics journal (2023) 100230.
[213] H.W. Loh, C.P. Ooi, S. Seoni, P.D. Barua, F. Molinari, U.R. Acharya, Application of explainable artificial intelligence for healthcare: a systematic review of the last decade (2011–2022), Comput. Methods Progr. Biomed. (2022) 107161.
[214] S.M. Lundberg, S.I. Lee, A unified approach to interpreting model predictions, Adv. Neural Inf. Process. Syst. 30 (2017).
[215] B. Zhou, A. Khosla, A. Lapedriza, A. Oliva, A. Torralba, Learning Deep Features for Discriminative Localization,, arXiv - Cs - CV, 2015, https://doi.org/10.48550/arXiv.1512.04150.
[216] M.T. Ribeiro, S. Singh, C. Guestrin, Why Should I Trust You?: Explaining the Predictions of Any Classifier, arXiv - cs - LG, 2016, https://doi.org/10.48550/arXiv.1602.04938.
[217] Harsha Nori, Samuel Jenkins, Paul Koch, Rich Caruana, Interpretml: A unified framework for machine learning interpretability, 2019 *arXiv preprint arXiv: 1909.09223*.
[218] G.R. Vasquez-Morales, S.M. Martinez-Monterrubio, P. Moreno-Ger, J.A. Recio-Garcia, Explainable prediction of chronic renal disease in the colombian population using neural networks and case-based reasoning, IEEE Access 7 (2019) 152900–152910, https://doi.org/10.1109/ACCESS.2019.2948430.
[219] Kourosh Kakhi, Roohallah Alizadehsani, H.M. Dipu Kabir, Abbas Khosravi, Saeid Nahavandi, U. Rajendra Acharya, The internet of medical things and artificial intelligence: trends, challenges, and opportunities, Biocybern. Biomed. Eng. 42 (3) (2022) 749–771, https://doi.org/10.1016/j.bbe.2022.05.008. ISSN 0208-5216.
[220] F. López-Martínez, E.R. Núñez-Valdez, R.G. Crespo, V. García-Díaz, An artificial neural network approach for predicting hypertension using NHANES data, Sci. Rep. 10 (1) (2020) 10620.
[221] Y. Hasanpoor, B. Tarvirdizadeh, K. Alipour, M. Ghamari, Stress Assessment with Convolutional Neural Network Using PPG Signals, in: 2022 10th RSI International Conference on Robotics and Mechatronics (ICRoM), IEEE, 2022, November, pp. 472–477.
[222] S. Lee, H.C. Lee, Y.S. Chu, S.W. Song, G.J. Ahn, H. Lee, S.B. Koh, Deep learning models for the prediction of intraoperative hypotension, Br. J. Anaesth. 126 (4) (2021) 808–817.
[223] W.H. Lin, F. Chen, Y. Geng, N. Ji, P. Fang, G. Li, Towards accurate estimation of cuffless and continuous blood pressure using multi-order derivative and multivariate photoplethysmogram features, Biomed. Signal Process Control 63 (2021) 102198.
[224] Y. Chen, D. Zhang, H.R. Karimi, C. Deng, W. Yin, A new deep learning framework based on blood pressure range constraint for continuous cuffless BP estimation, Neural Network. 152 (2022) 181–190.
[225] Q. Hu, D. Wang, C. Yang, PPG-based blood pressure estimation can benefit from scalable multi-scale fusion neural networks and multi-task learning, Biomed. Signal Process Control 78 (2022) 103891.
[226] S. Liu, Z. Huang, J. Zhu, B. Liu, P. Zhou, Continuous blood pressure monitoring using photoplethysmography and electrocardiogram signals by random forest feature selection and GWO-GBRT prediction model, Biomed. Signal Process Control (2023) 105354.
[227] F. Shoeibi, E. Najafiaghdam, A. Ebrahimi, Nonlinear features of photoplethysmography signals for Non-invasive blood pressure estimation, Biomed. Signal Process Control 85 (2023) 105067.
[228] T. Sadad, S.A.C. Bukhari, A. Munir, A. Ghani, A.M. El-Sherbeeny, H.T. Rauf, Detection of cardiovascular disease based on PPG signals using machine learning with cloud computing, Comput. Intell. Neurosci. 2022 (2022) 11, 1672677.
[229] M. Simjanoska, S. Kochev, J. Tanevski, A.M. Bogdanova, G. Papa, T. Eftimov, Multi-level information fusion for learning a blood pressure predictive model using sensor data, Inf. Fusion 58 (2020) 24–39.
[230] M. Alkhodari, D.K. Islayem, F.A. Alskafi, A.H. Khandoker, Predicting hypertensive patients with higher risk of developing vascular events using heart rate variability and machine learning, IEEE Access 8 (2020) 192727–192739, https://doi.org/10.1109/ACCESS.2020.3033004.
[231] Y. Liang, Z. Chen, G. Liu, M. Elgendi, A new, short-recorded photoplethysmogram dataset for blood pressure monitoring in China, Sci. Data 5 (1) (2018) 1–7.
[232] X.L. Zou, Y. Ren, D.Y. Feng, X.Q. He, Y.F. Guo, H.L. Yang, T.T. Zhang, A promising approach for screening pulmonary hypertension based on frontal chest radiographs using deep learning: a retrospective study, PLoS One 15 (7) (2020) e0236378.